A Master's Thesis Submitted to the Department of Oceanography in the School of Ocean and Science and Technology

Degree: Master of Science in Oceanography

Date of Graduation: Spring 2023

Committee Members:

Angelicque White (chairperson)
Seth Bushinsky
James Potemra
David Ho

Title:

Chlorophyll Bloom Dynamics and Associations with Mesoscale and Submesoscale Features in the North Pacific Subtropical Gyre

Author: James Ash

1. ABSTRACT

Large summer chlorophyll blooms spanning hundreds of square kilometers and persisting for weeks-months, are consistently observed in satellite records of the Northeast Pacific Subtropical Gyre (NPSG), at an approximate latitude of ~30°N. These blooms occur at a near annual rate, and uniquely within the late summer months of June-October. Understanding the potential impacts and biophysical drivers of these chlorophyll anomalies is both ecologically and climatologically important. These large-scale blooms can export carbon from the upper ocean to the deep ocean and fuel the productive fisheries found in the ecologically important transition zone between the North Pacific Subtropical Gyre and the subpolar gyre.

The purpose of this project is to characterize chlorophyll blooms in the NE Pacific Gyre, as well as describe their association with submesoscale and mesoscale features to identify potential physical drivers. First, an analysis of the merged satellite CHL product is done to characterize the magnitude, frequency, and geographic location of chlorophyll blooms in the NPSG. Then the sea level anomaly (SLA) and finite sized Lyapunov exponents (FSLE) were used to identify sub-mesoscale and mesoscale features i.e. fronts, anti-cyclonic eddies, and cyclonic eddies. Through this process, we provide a quantitative characterization of chlorophyll anomalies in the NPSG. Further analyses present a case-study time-series of the 2018 bloom in order to better understand the time-resolved change in phytoplankton biomass and how it relates to physical drivers of biomass growth and accumulation. To achieve this, a generalized additive model (GAM) is used to determine the effects of SLA and SSTA on the CHL anomaly signal of the 2018 plankton bloom.

2. TABLE OF CONTENTS

3. INTRODUCTION

Some of the earliest ecological studies in the oceans have focused on mechanisms that drive rapid growth and accumulation of bulk phytoplankton biomass and/or distinct phylogenetic groups: e.g. the spring bloom of diatoms in the North Atlantic (Sverdrup 1953), aperiodic blooms of the diazotroph *Trichodesmium* that can lead to visually striking surface slicks (Mohler 1941, Capone et al. 1998), and harmful algal blooms that can bioaccumulate in marine food webs and impact human health (LoCicero 1974). These phenomena are areas of intense study, as shifts in phytoplankton biomass can alter microbial interactions, trophic structure, elemental fluxes from the epipelagic to the mesopelagic, and other aspects of ocean ecology. The spatial and temporal scales of phytoplankton blooms can vary from days to weeks and from narrow windows of biomass to km^2 scale patches (Liu 2016, Siswanto 2016). The definition of a bloom however is not universal; as described by Smayda (1997): "what constitutes a bloom…has regional, seasonal, and species-specific aspects; it is not simply a biomass issue." This is clear when considering the relatively low variation of phytoplankton biomass estimates within the oligotrophic subtropical gyres that occupy ~40% of the global surface area (Karl 2002). In the North Pacific Subtropical Gyre (NPSG, Figure 1), the seasonal mean range in chlorophyll, used as a proxy for phytoplankton biomass, in the near surface waters is only ~0.15 mg m^{-3} (White et al. 2007, Karl et al. 2021) as measured by the Hawaii Ocean Time-series (HOT) at Station ALOHA (A Long-term Oligotrophic Habitat Assessment, 22.75°N, 158°W) Much of this seasonality is driven by photoacclimation, where phytoplankton modify their cellular pigment concentrations in response to the seasonal cycle of insolation (Campbell et al. 1997, Graff et al. 2016). This relatively low seasonality in surface phytoplankton biomass led to earlier conceptualization of the NPSG and other

subtropical gyres as 'ocean deserts' Irwin and Oliver (2009) typified by 'endless summer' (Venrick 1993).

The HOT program has sampled the NPSG at Station ALOHA at near monthly intervals since 1988, and found that blooms (enhanced chlorophyll or specific classes of organisms) are generally confined to summer months and often associated with nitrogen-fixing organisms (diazotrophs). In 1996, a transect from Station ALOHA to the Climax area (28°N) utilizing a towed underway system sampling at 45 m, observed a large bloom spanning ~250 m with peak chlorophyll concentrations of ~0.4 mg m^{-3}. Net tows along this transect revealed high concentrations of the diazotroph *Trichodesmium* and pigment analyses indicated high levels of the diatom pigment-marker fucoxanthin, perhaps pointing to the growth of diatom-diazotroph assemblages, DDAs (Dore et al. 2008). This finding is not atypical as blooms of *Trichodesmium* are frequently reported at or near Station ALOHA (Marumo & Asaoka 1974, Gundersen et al. 1976, Mague et al. 1977, Letelier & Karl 1996). Later, Fong et al. (2008) observed surface chlorophyll ranging from 0.2-0.4 mg m^{-3} within an anticyclonic eddy near Station ALOHA. Sampling of this feature revealed a high concentration of an assortment of N_2-fixing organisms. In addition to observations of elevated concentrations of diazotrophs in summer at Station ALOHA, there are also documented pulses of particle export to the deep sea in the summer months that have been attributed to shifts in the microbial community to favor DDAs (Karl et al. 2012). Overlying the seasonality of export productivity at this location are long term trends; Karl et al. (2021) report a 30-yr long increase in chlorophyll, suspended particulate carbon and nitrogen, and primary production at Station ALOHA. The proposed drivers of these oligotrophic summer blooms (and associated particle flux) include enhanced iron

flux (Capone et al. 1998), physical aggregation of buoyant cells (such as *Trichodesmium*) (Mohler 1941), and nutrient intrusions into the euphotic zone via mesoscale eddy pumping (Dore et al. 2008, Karl et al. 2012). These late summer chlorophyll blooms do not seem to be correlated with sea surface height anomalies or wind forcing, but this has not been rigorously tested (White et al. 2007, Friedrich et al. 2021).

To the north of Station ALOHA, large summer blooms of satellite-derived chlorophyll (CHL) spanning hundreds of square kilometers and persisting for weeks to months, are consistently observed in satellite records at an approximate latitude of ~30°N (Wilson 2013) in the NE region of the NPSG (here termed NEPSG). These blooms have been operationally defined as having a CHL value greater than 0.15 mg m^{-3}, which is ~3× greater than the background CHL level of 0.05 mg m^{-3} for the oligotrophic oceans (Villareal 2011, Wilson 2013, Toyoda & Okamoto 2017). These blooms occur at a near annual rate, and uniquely within the late summer/early fall months of June-October (Wilson 2003, 2008, 2011, 2013).

Remote sensing of ocean color was first used to describe these CHL blooms in 2003 through the use of the Sea-viewing Wide Field-of-view Sensor (SeaWiFS) ocean color satellite (O'Reilly 2000, Wilson 2003). In 2002, Wilson et al. serendipitously sampled a phytoplankton bloom in the NEPSG region and observed an elevated abundance of the diazotrophs, *Trichodesmium* and *Rhizosolenia* (a diatom that can harbor the diazotroph *Richelia*) (Wilson 2003). Later studies have attempted to characterize the biological and physical components of the NEPSG blooms (Wilson 2008, Villareal 2011, Wilson 2013, Lehahn et al. 2017, Toyoda & Okamoto 2017), but to date, no one system of biophysical drivers has been conclusively established. Currently, there are six inter-related

hypotheses as to the cause of observed annual phytoplankton blooms in the NEPSG; these include (i) stimulation of di-nitrogen fixing bacteria via iron or phosphorus inputs during warm and well-stratified summer months (Follett et al. 2018), (ii) inputs of nitrate from vertically migrating mats of the diatom *Rhizosolenia* (Wilson 2003, 2008), (iii) nitrate inputs into the euphotic zone via breaking of internal waves or subsurface mixing (Letelier et al. 2000, Wilson 2008), (iv) the entrainment of nutrient rich deep water into the mixed layer driven by an increase in Ekman transport across a northward sea surface salinity gradient (Wilson 2003, Wilson & Coles 2005, Wilson 2013, Toyoda & Okamoto 2017), and (v) regulation of horizontal dilution rates which may impact the balance of phytoplankton growth and grazing rates (Lehahn et al. 2017). Lastly, the NPSG is generally an area of converging surface currents which is conducive for the aggregation of buoyant phytoplankton (Wilson 2013), leading to (vi): these 'blooms' may not result from local growth but rather a concentration of living biomass along surface current fronts. The majority of these mechanisms requires some physical mechanism (oceanic or atmospheric) of enhancing nutrient delivery to the surface mixed layer or concentrating biomass that is then observable by satellites.

From a bottom-up perspective, large mesoscale eddies and submesoscale flows in the open ocean can both induce vertical and horizontal motion, leading to oscillations of isopycnals which may influence plankton biogeochemistry through changes in the distributions of nutrients within the euphotic zone. In cyclonic eddies for example, isopycnal layers are uplifted, inducing upwelling at the eddy's core which can enhance the supply of growth-limiting inorganic nutrients into the well-lit upper ocean. Conversely, in anticyclonic eddies isopycnal layers are depressed, inducing down-welling at the

eddy's core and driving deepening of nutrients at the surface ocean (McGillicuddy Jr & Robinson 1997, Hernández-Carrasco 2011, Hernández-Hernández et al. 2020). In the oligotrophic NPSG as well as the North Atlantic, anticyclonic eddies have been observed in conjunction with elevated N_2 fixation rates and/or elevated concentrations of N_2 fixing organisms (Fong et al. 2008, Church et al. 2009, Dore et al. 2016) although as Dore et al. (2008) noted at the time "the exact physical, biogeochemical, and ecological processes underlying this apparent mesoscale stimulation of diazotroph activity in the oligotrophic ocean have yet to be identified."

How might mesoscale eddies lead to enhanced phytoplankton biomass and what is the evidence for such drivers in the NPSG? The work of Guidi et al. (2012) and Wilson (2021) provide some observations and hypotheses. In 2008, Guidi et al. (2012) combined high-resolution biogeochemical and physical data sets to examine the evolution of a *Trichodesmium* bloom occurring in the frontal transition zone between a weak anticyclonic and cyclonic eddy near Station ALOHA. They argue that the interaction between the two eddies generated horizontal stirring, i.e. sub-mesoscale frontal regions, that controlled the distribution of phytoplankton biomass leading to elevated chlorophyll a, particle concentrations, and export flux in the frontal region where *Trichodesmium* concentrations were elevated. Specifically, the sub-mesoscale frontal effects are two-fold, (i) the upward component of sub-mesoscale fronts can transport nutrients into the euphotic zone enhancing phytoplankton growth, while (ii) the downward component can subduct phytoplankton below the euphotic zone into the subsurface and ultimately drive biomass export into the deep ocean. Wilson (2021) presents Biogeochemical-Argo float data near 30°N and argues that cyclonic eddies play an important role in mesoscale nitrate shoaling

events (and hence injections of nitrate to the lower euphotic zone). In that study, most of these nitracline shoaling events (7 of 8) were associated with cyclonic eddies during phases of eddy shedding, merging, or during periods when eddy speed changed significantly (Wilson 2021). These nitrate injection events were followed by increased surface chlorophyll, although it is not clear how or whether these deep perturbations reached the surface mixed layer.

Similarly, turbulent mixing driven by baroclinic instabilities is another element in the set of bottom-up perspectives on phytoplankton growth. Uniquely in the NEPSG, the generation of semi-diurnal internal waves by tidal flow over the Hawaiian Ridge system is an important pathway for the conversion of tidal energy into oceanic mixing (Rudnick et al. 2003, MacKinnon & Winters 2005, Klymak et al. 2006), and subsequent large-scale open ocean phytoplankton blooms (Wilson 2011). Internal waves generated along the Hawaiian ridge system radiate outward into the surrounding ocean, and their associated energy can be an order of magnitude larger than internal waves typically observed in the open ocean (Klymak et al. 2006). The dissipation of these internal waves into the upper ocean can create hotspots of mixing where mid-ocean water is entrained into the surface ocean layer nearly 1000 km away from the site of the internal wave generation (MacKinnon & Winters 2005, Klymak et al. 2006). Mode water thus entrained can be a vital source of nutrients to the surface ocean, and drive large-scale open ocean plankton blooms (Wilson 2011). Specifically, much of the tidal energy that interacts with the Hawaiian Ridge system decomposes through subharmonic instabilities that drive surface mixing at the critical 30°N latitude, where mesoscale chlorophyll blooms are observed on a near annual basis (MacKinnon & Winters 2005).

From a top-down perspective, Lehahn et al. (2017) used a simple ecosystem model to show that once a bloom has been initiated, the dispersion of fine scale nutrient enriched water may regulate the predator-prey encounter rate between phytoplankton and zooplankton within the ecosystem, and lead to net biomass accumulation in excess of losses. Lehahn et al.'s proposed pathway ultimately enhances the accumulation of photosynthetic biomass in low nutrient oceanic environments, such as the NEPSG. Furthermore, the spatial structure of the 2007 bloom, that occurred within the NEPSG, was recreated by seeding points within the initial bloom contours, and allowing the points to disperse via geostrophic surface flows, with plankton dynamics simulated with a simplified ecosystem model. This provides evidence that blooms in this region are initiated by a nutrient seeding event, and phytoplankton growth is then the result of a top-down trophic cascade (Lehahn et al. 2017).

While many of the past studies of bloom dynamics in the NPSG/NEPSG have focused on the potential biophysical drivers of phytoplankton blooms using a threshold approach, (e.g. CHL> 0.15 mg m^{-3} is defined as a bloom), none have explicitly addressed the fact that seasonal photoacclimation is a strong component of the chlorophyll signal in the subtropics (Campbell et al. 1997, Graff et al. 2016). The process of photo-acclimation, where phytoplankton modify their cellular pigment concentrations in response to the seasonal cycle of insolation, leads to lower mean chlorophyll values in summer months with the highest irradiance and highest mean chlorophyll in lower light winter months.

The purpose of this study is to characterize seasonally-detrended CHL anomalies within the NPSG/NESPG region including the 30°N critical latitude (Figure 1) where

canonical summer blooms have been reported (Wilson 2003, 2013) and at Station ALOHA. We characterize the magnitude, frequency, and persistence of CHL blooms in these regions and quantitatively examine associations of these blooms with mesoscale and sub-mesoscale features to identify potential physical drivers of CHL anomalies. We perform a cluster analysis using sea level anomaly (SLA) fields in conjunction with FSLE fields to determine a spatial association between anomalous CHL and mesoscale and submesoscale features, following the methods outlined in Guo et al. (2019) in order to determine the relative association of mesoscale and sub-mesoscale regions with CHL patterns for each of the bloom region. Lastly, we present a case-study time-series of the 2018 CHL bloom observed in the NEPSG in order to better understand the time-resolved change in phytoplankton biomass and how it relates to chemical and physical drivers of biomass growth and accumulation.

4. METHODS
A. DATASETS

Finite Sized Lyapunov Exponent (FSLE) fields (4 km spatial resolution, 1-day temporal resolution) were obtained from the Archiving, Validation, and Interpretation of Satellite Oceanographic data (AVISO) web server. Sea Level Anomaly (SLA) fields (4 km, 1-day resolution) were downloaded from the Copernicus Marine Server (CMEMS). All eddy related parameters including type, amplitude, radius, and lifetime from the Mesoscale Eddy Trajectory Atlas (META) product were accessed through AVISO's THREDDS server. Satellite chlorophyll (CHL) from Global Ocean Colour (Copernicus-GlobColour) were accessed via the copernicus data portal's THREDDS server. The specific CHL data set used were the GlobColour 1-day and 8-day 4-km resolution (data-set id: OCEANCOLOUR_GLO_BGC_L3_MY_009_103). GHRSST level 4 MUR sea surface

temperature analysis (SSTA) data were accessed through NOAA's ERDDAP server. The date range of the SLA, FSLE, and SSTA satellite data downloaded was from January 06, 2002 to January 01, 2022. The date range of the CHL satellite data downloaded was from January 06, 1997 to December 31, 2022.

Here we use the term mesoscale to describe any physical feature that occurs on the order of one month in time and within 10 km^2 to 200 km^2 in size. An eddy is then defined as a mesoscale feature that experiences high rates of strain and is composed of two parts: a region of high vorticity known as the core, surrounded by a circulation cell known as the ring (Flierl & McGillicuddy 2002). The submesoscale describes any physical feature less than 10 km in size and is representative of current fronts associated with twisting and stretching.

Submesoscale and mesoscale features are identified using the FSLE fields, and SLA fields (Guo 2019). FSLE is defined as the inverse time of the separation of two particles from their initial distance to their final distance. To identify submesoscale regions in FSLE and SLA fields, and correlate the CHL product to submesoscale features, the CHL and SLA products are re-sampled to the FSLE grid using a nearest neighbor interpolation, i.e. each output grid cell is an interpolation of the nearest 2×2 grid cells from the original CHL and SLA matrices, respectively. Similarly, this was done between CHL, SLA, and SSTA for application in the generalized additive model, where SSTA and SLA where resized to CHL using the nearest neighbor method.

In order to validate the CHL product, in situ HPLC chlorophyll (high-pressure liquid chromatography) data from the upper mixed layer (0 – 25 m), were downloaded directly from the Hawaii Ocean Time-series ftp web server; these data are at near monthly

resolution. The geometric mean of a 3×3-pixel region (12 ×12 km) around Station ALOHA was subset from the CHL time-series and matched by time-stamp (± 1 day) to the HPLC CHL data; a linear regression between HPLC and the CHL product was performed (Figure 2).

B. STUDY REGION AND SUMMARY STATISTICS

We have defined one distinct study region centered at 150°W and 28°N with longitude and latitude boundaries of 170°W-130°W, 18°N-38°N. This encompasses Station ALOHA, the main Hawaiian island chain, the critical latitude at 30°N, and the easternmost part of the North Pacific transition zone. Generally, Station ALOHA is not impacted by the seasonal migration of the North Pacific transition zone, while the northern most sections of the study region are impacted by the North Pacific transition zone and exhibit strong interannual variability (Villareal 2011, Wilson 2011, 2013, Toyoda & Okamoto 2017). Importantly we also remove the interannual variability within the CHL signal to produce a CHLA signal that simultaneously removes the northward chlorophyll gradient. This allows us to examine relationships between CHLA, FSLE, and SLA fields at every gridded point within the study region. We also remove the coastal regions around the main Hawaiian Islands, using the states exclusive economic zone (EEZ) zone as a special polygon to clip the satellite data.

The bloom region was chosen by taking similar longitude/latitude boundaries to those described in Wilson (2013), but extending the latitude range southward to include the blooms occurring at Station ALOHA. The southward latitude boundary was chosen by producing a contour map of the late summer CHL climatology (Figure 1) in the NPSG, and choosing a boundary that encompasses all large plankton bloom features. Defining

the bloom study region in this way is ultimately subjective, and there are slight variations in the region boundaries compared to previous studies (Wilson 2013, Toyoda & Okamoto 2017), but this choice allows us to focus on a single central bloom region. Furthermore, the boxes are defined only to mark general bloom regions, and are used to determine the frequency of bloom occurrences, but the subsequent statistical analysis is not heavily dependent on the box boundaries (data not shown), and the box coordinates are given for reproducibility.

The monthly mean climatology for a 12 × 12 km region around Station ALOHA was also calculated for both the CHL and HPLC chlorophyll (Figures 1, 2). Based on this climatology, we have focused on the late summer months (July - October) of each time-series where blooms are more apparent. This temporal window is consistent with the approach of Wilson et al. (2011, 2021) which observed blooms to be roughly restricted to June-October. To capture the peak of the late summer CHL blooms, only SLA, FSLE, CHL, and CHLA data from July-October were used in all the succeeding statistical analyses.

The bloom start and end dates were found by viewing weekly chlorophyll contour maps of the study region within the late summer months. The bloom durations were found by subtracting the bloom end dates from the bloom start dates (Figure 3). The bloom magnitude was defined as the maximum value CHL concentrations reached at any point during the bloom's lifespan (Table 1, Figure 4). The bloom area was calculated as the maximum area the bloom reached across the bloom's lifespan (Table 1, Figure 4). The bloom center coordinates were found by finding the longitude and latitude location where each bloom reached its greatest chlorophyll concentration, on the day the bloom reached

its maximum area (Table 1). To mitigate the effects of clouds, the 8-day CHL product was used to find the bloom areas and center. To visualize the bloom's location and area, circles were mapped with their center coordinates corresponding to the coordinates of the bloom's center, and whose area corresponds to the maximum area that the blooms reached (Figure 5).

C. DEFINING A BLOOM

To remove the seasonal and climate signal from the CHL product and define CHLA, the seasonal monthly median and long-term climate signal were subtracted from each grid cell of the CHL field. This is because the total CHL signal can be thought of as the sum of three parts. Those are the seasonal trend S_t, the climate trend C_t, and the residuals R_t, such that

$$CHL = S_t + C_t + R_t$$

To be clear, we use the term "climatological signal" to represent the long-term deviation from the typical seasonal patterns. Usually the term climatological refers to the mean seasonal cycle. Here we treat the seasonal signal and the climatological signal separately, and consider the time domain of the climatological signal to extend across the entirety of the data set, 1997-2022.

The seasonal signal was found by calculating the median of the entire CHL dataset grouped by each month, resulting in a twelve-layer raster object, with each layer corresponding to the twelve months of the year. The seasonal signal was removed from the CHL dataset by subtracting each daily layer of the CHL dataset by its respective monthly average within the S_t product. The climatological signal was found using running polynomial regression on each of the grid cells of the CHL dataset, resulting in a raster

14

object C_t, with the same dimensions as the CHL dataset. The climatological signal was then subtracted directly from the CHL dataset using typical matrix arithmetic.

$$R_t = CHL - S_t - C_t$$

While generally an anomaly is defined as outliers of a dataset, in geographic data sets an anomaly is traditionally defined as the deviation from a background signal i.e. the residuals. Here the background signal is defined as S_t and C_t. Therefore, the seasonally filtered CHL anomaly (CHLA) is the residuals of the CHL product.

$$CHLA = R_t$$

A bloom threshold was then defined as the median plus the mean absolute deviation (MAD) for each grid cell across the length of the data set of the R_t fields. Bloom values were defined as chlorophyll values that were greater than the bloom threshold i.e. the positive anomaly. A raster mask of bloom flags was saved to be used in future analysis of bloom persistence and spatial scale.

To depict the general location of blooms in the study region, the CHLA for the late summer months across the entire data set (1997 - 2022) was averaged and mapped (Figure 1). Then, to visualize the yearly bloom occurrences, monthly thumbnail plots of the bloom values were produced (Figure 6). Bloom values were identified in the daily CHLA as described, and summed over a monthly period for the late summer (June - October). For this analysis, bloom years that spanned the largest area were chosen to be displayed (Table 1, Figure 5).

D. IDENTIFYING SUBMESOSCALE REGIONS

A Veroni decomposition was applied to the yearly (late-summer only) SLA and FSLE fields within the study region to group the parameters into submesoscale categories, and a percent association to chlorophyll bloom values is derived for each submesoscale group (Ogniewicz & Kübler 1995) (Figure 7). We employed a similar approach to that outlined by Gou et al. (2019) where a k-means clustering algorithm (k = 4) is used to group the SLA and FSLE data points into one of four physical regions based on the cluster's centroid location in FSLE-SLA space (Figure 7) i.e. positive mesoscale, negative mesoscale, sub-mesoscale and mixed. Here, we do not use a k-means cluster algorithm, but do group the points based on the nearest distance to center locations. Where a k-means cluster algorithm determines the centers using a stochastic process, and the centers were chosen based on the mean and standard deviations of the FSLE and SLA as described below.

To achieve this, the FSLE and SLA gridded fields are scaled from 0 to 1. The inputs of the Veroni decomposition are FSLE and SLA, and for each FSLE and SLA pair in space and time, the output is a submesoscale group factor of 1, 2, 3, or 4. The group centers of the Veroni decomposing were set using the mean and standard deviations of the SLA and FSLE fields (Figure 7). These four groups each represent the four physical regions of the ocean's surface. The coordinates of the mesoscale positive, mesoscale negative, sub-mesoscale, and mixed fields are $((u_s+o_s, u_f), (u_s-o_s, u_f), (u_s+o_s, u_f), (u_s-o_s, u_f))$ respectively. Where u_s and o_s are the mean and standard deviation of the SLA field, and u_f and o_s are the mean and standard deviation of the FSLE field. For display purposes

the submesoscale groups identified this way are re-gridded into latitude and longitude space (Figure 8), and a single day, 2018-06-01, of the study region is displayed as a map.

To determine the association of the CHL blooms with the submesoscale regions, the percent of CHL bloom data points grouped in each submesoscale region was calculated by year. So that percent association represents the increased or decreased probability of a bloom value occurring within a submesoscale feature; the percent association was found similarly to a percent error calculation, such that

$$Percent\ Association\ = \ |\frac{blooms - background}{background}| \ \ \times 100\ [\%]$$

Where *blooms* are the observed amount of bloom values associated with submesoscale features, and the *background* is the expected amount of bloom values associated with submesoscale features. For all blooms that occurred during the late summer months, between the years 2002 and 2020, the output of the Veroni decomposition and the percent association to submesoscale regions is shown in Figure 7. Similarly, CHLA is mapped to an FSLE and SLA grid using the nearest neighbor method, and plotted as a contour plot with the CHLA value as color. Each grid cell color is found as the median CHLA value corresponding to that FSLE and SLA in space and time (Figure 7).

To show the general association between eddies and fronts to satellite chlorophyll, outer eddy contours from the META dataset were plotted over the bloom values from the 2019 and 2020 blooms (Figure 9). Cyclonic eddies are depicted with black polygons, and anticyclonic eddies are depicted with gray polygons. Similarly, to show the association of frontal features to the chlorophyll satellite product, the bloom values were plotted over

17

FSLE contours (Figure 9). For this, the daily cloud-free chlorophyll satellite product was used so that the bloom snapshots could be compared to the more ephemeral eddy contours and frontal features.

E. CASE STUDY OF THE 2018 BLOOM

To show the association of the 2018 bloom with frontal features, fronts identified using FSLE fields were plotted alongside the 2018 bloom feature. For visualization purposes, frontal features were identified as any FSLE values above the median plus the MAD of the daily FSLE field. Then the chlorophyll anomaly was calculated and bloom values were identified as described before, and displayed as a scatter plot (Figure 10). For this the 8-day CHL downloaded directly from the NOAA ERDDAP server (ID: erdMH1chla8day), was used.

To show that the 2018 bloom occurred with massive earthquake events, a CHLA timeseries at Station ALOHA was plotted alongside a timeseries of earthquake occurrences along the Hawaiian ridge (Figure 11). For this, over 23 years of earthquake and CHLA data were monthly averaged. Earthquake data was downloaded directly from the United States Geological Survey's web server. A region around the Hawaiian ridge was used as the boundary to select for earthquakes that could be associated with eruptions, and that have an impact on regional marine life. Specifically, earthquakes greater that magnitude 3, between 1996-10-01 to 2023-01-20, and within the extent (162°W, 154°W, 18°N, 2°3N) were selected. For the CHLA data, a 3-pixel region around Station ALOHA was used.

To determine the effect mesoscale eddy pumping may have on the chlorophyll concentration within the 2018 bloom, a generalized additive model (GAM) was applied to

the CHLA, SLA, and SSTA data sets. Within the GAM, the daily GlobColor satellite chlorophyll anomaly was input as the response variable, and the SLA and SSTA were the predictor variables. To account for the northward CHL gradient and seasonal photoacclimation signal, time and space (longitude/latitude) were input as smoothers within the GAM (Figure 12). The response variable, CHL, was modeled as a draw from a gamma distribution and a restricted likelihood (RELM) smoothing parameter estimation method was chosen. The zero eddy amplitudes that generally separates cyclonic and anticyclonic regions are shown as the vertical black lines (Figure 12).

To directly compare SSTA and CHL, a map of a single day was created near the peak of the 2018 phytoplankton bloom. The date 2018-09-17 was chosen to display, because a large and distinct branch of warm surface water was visible in the SSTA signal, that aligned with an increased in the CHL signal (Figure 13). It should be noted that nearly every day during the 2018 phytoplankton bloom showed signs of SSTA fronts aligning with CHL fronts, but the event observed on 2018-09-17 was the most drastic. To show that the center of the 2018 phytoplankton bloom aligned with a strong temperature anomaly gradient, Hovmöller plots where generated (Figure 14) using SSTA and CHL over the region 155 to 130°W, 18-35°N and across the time span of 2018-08-01 – 2018-08. For reference, a black vertical line was plotted along the latitude of Station ALOHA, near the Hawaiian Islands.

Daily surface area, integrated chlorophyll biomass, and chlorophyll concentration were calculated using the methods outlined in Lehahn et al (2017). The chlorophyll concentration was found as the mean chlorophyll signal over the daily surface area of the bloom patch. Chlorophyll biomass was found by integrating the chlorophyll concentration

across daily estimates of the mixed layer depth. The mixed layer depth was found by applying the calculation derived by Chu and Fan (2011) to Argo-float depth profiles of salinity and temperature (density). The area was found by calculating the daily total area of the bloom (Figure 15), with bloom values identified using the threshold method described previously.

The mixed layer depth in conjunction with the daily bloom area estimates (Figure 15), and chlorophyll concentration [mg m^{-3}] was used to calculate daily bloom biomass [tons] (Figure 15). To do this, surface satellite chlorophyll [mg m^{-3}] observations were assumed to be uniformly distributed throughout the mixed layer. Then the chlorophyll concentration was integrated spatially across its cartesian coordinates i.e. longitude and latitude, and vertically across the mixed layer depth (Lehahn et al. 2017). Specifically, the daily bloom area, mixed layer depth, and average chlorophyll concentration were found, then the biomass was calculated as the product of the daily bloom area, mixed layer depth, and average chlorophyll concentration.

RESULTS
A. GLOBCOLOR CHL AS A PROXY FOR PHYTOPLANKTON CONCENTRATION

Validation of the CHL product was performed versus in situ HPLC-derived chlorophyll from the HOT program. By directly comparing co-occurring measurements of HPLC to CHL, we find a significant linear relationship ($p < 0.05$, $n = 223$, Figure 2). When comparing monthly grouped averages of HPLC and CHL, we find CHL well approximated the seasonal cycle at Station ALOHA (Figure 2). This gives a measure of confidence for the regional CHL and derivation of bloom events. The seasonal trend of HPLC and CHL are similar with strong agreement in the summer to early winter, which covers the time

domain of this project; the greatest deviation of HPLC from CHL occurred in the late winter months (Figure 2). There are however observations of mesoscale phytoplankton blooms that were not apparent in the HPLC bottle samples (223 total bottle samples). This is possibly due to the lower temporal resolution of HPLC bottle samples (~monthly) compared to the daily coverage GlobColour CH1L satellite product and bloom patchiness in space and time.

Both in situ HPLC chlorophyll and satellite CHL reveal strong seasonality at Station ALOHA with pigment concentrations driven by photo-acclimation (Figure 2). In winter months when incoming irradiance and day length is at their minimum, chlorophyll concentrations are highest. Inversely, in the summer when irradiance is at its maximum, chlorophyll concentrations are minimal. This trend reflects the regulation of cellular pigment concentrations to optimize growth (Graff et al. 2016); and is also seen when examining chlorophyll per cell for the abundant photoautotroph *Prochlorococcus* (Campbell et al. 1994). This seasonal photo-acclimation is removed from the time-series when calculating anomalies (Figure 1).

B. CHARACTERIZING PHYTOPLANKTON BLOOMS

Chlorophyll blooms with an area greater than 4×10^5 km^2 occur every year within the NEPSG. Large scale chlorophyll blooms greater than 10×10^5 km^2 in size occur nearly annually within the study region, both at 30°N and Station ALOHA. Across the 22 years of interest, from 1997 to 2022, 13 large scale phytoplankton bloom events occurred. Six of these blooms occurred near Station ALOHA just north of the main Hawaiian Islands (1997, 2009, 2010, 2013, 2015, 2018) and seven occurred near 30°N (2003, 2004, 2008, 2011, 2014, 2019, 2020) with five of these blooms spanning across the entire study region

(2006, 2014, 2015, 2018, 2020). The five blooms that occurred at Station ALOHA, excluding 2018, stayed within a latitudinal range of 20°N to 28°N. Of the seven large blooms that occurred at 30°N, three centered along -160°W (2007, 2011, and 2020), and three centered along -140W (2003, 2004, 2019). Of all the blooms, the maximum CHL signal ranged from 0.14 mg m^{-3} (2021) to 1.42 mg m^{-3} (2010), with an average of 0.57 mg m^{-3}, approximately 11.4 times the background signal of 0.05 mg m^{-3}. The minimum duration was 37 days (2017) and the maximum bloom duration was 131 days (2020).

C. ASSOCIATION OF SUB-MESOSCALE FEATURES TO PHYTOPLANKTON BLOOMS

The background signal of eddies and fronts identified using one standard deviation of the FSLE and SLA data sets was as follows. Cyclonic features composed 25.0% of the geographic area, and anti-cyclonic features composed 23.7% of the geographic area for a total percent area cover of 48.7% (Figure 7). Frontal features composed 7.34% of the geographic area. Lastly, mixed regions composed 43.9% of the area covered (Figure 7). This agrees with METAP eddy area coverage of roughly 45% for both cyclonic and anticyclonic eddies (Fu 2009) in the region. The background signal of strong eddies and fronts, that were identified using *two* standard deviation of the FSLE and SLA data sets, was as follows. Frontal features composed 15% of the geographic area, strong cyclonic eddies compose 16% of the geographic area, and strong anti-cyclonic eddies composed 16% of the geographic area.

When viewing CHLA mapped to the FSLE-SLA grid, generally mixed regions have little effect on CHLA with more extreme values of CHLA occurring with more extreme values of SLA and FSLE. We found no obvious linear trend between CHLA and SLA or FSLE for our region in the North East Pacific Subtropical Gyre.

The result of the percent association between CHL bloom values and submesoscale features is shown in Figure 7. Across all years, there was a positive association with anticyclonic features (positive mesoscale features) with an average association of 7.5%. The most positive association with anticyclonic features was nearly 23.2% in 2005, and the most negative association was nearly -19.1% in 2009. Generally, there was a negative association with cyclonic features (negative mesoscale) with an average of -11.5%. The most positive association with cyclonic features occurred in 2009 at 22.1%, and the most negative association occurred in 2021 at -34.9%. Across all years, 2002-2022, bloom values were positively associated with frontal features with an average association of 6.6%. The year with the most positive association occurred in 2015 with 11%, and the most negative association occurring in 2014 with -19.6%. Overall, there was very small association to mixed regions, with an average association of 0.3%.

D. CASE STUDY OF THE 2018 BLOOM

The 2018 bloom began on July 16th and persisted until November 5th. At first, it appeared as a patchy feature within the mesoscale size range along the 30°N line. At this time a frontal filament of chlorophyll branched off of the island of Hawai'i, originating near the Kamaʻehuakanaloa seamount, and spiraled north until it merged with a larger, newly developed CHL bloom feature (Wilson et al. 2019). For the first half of the bloom's lifespan, it persisted as two separate features, with one central mass along 30°N and the other further south near Station ALOHA. On September 2nd the bloom reached its maximum intensity, with the two features merging to create one large bloom feature, that spanned from 18°N to 35°N. After September 26th the bloom appeared to dissipate, with the few last remaining mesoscale chlorophyll features remaining along the 30°N line until

November 5th. Generally, the 2018 bloom appeared to be associated with frontal features across its entire lifespan (Figure 10).

Through the application of a generalized additive model we found a significant effect of SLA and SSTA on CHL ($p > 0.05$). The total deviance explained between SLA and SSTA, time, and space (longitude and latitude) smoothers was 30.7%. For the second GAM between SSTA, SLA, time, and space (longitude and latitude) smoothers, the total variance explained was 32.6%. Generally, positive SLA features had a positive effect on CHL, while negative SLA features had a slightly negative effect on CHL (Figure 7). For the second GAM, negative SLA had a negative effect on SSTA, and positive SLA had a variable effect on SSTA anomaly (Figure 7).

Throughout the lifespan of the bloom there was a visible association to SSTA fronts given by observation of SSTA and CHL maps (Figure 13). While only the day 2018-09-17 is shown, this association is apparent from the beginning to the demise of the 2018 phytoplankton bloom. Similarly, the center of the 2018 bloom occurs along the latitude of 25°N. This coincides with a strong temperature anomaly gradient spanning the latitudes of 22°N to 26°N (Figure 14).

Within the 2018 bloom period, the mixed layer depth averaged 32 m, with a slight shoaling in mid-late August based on the mixed layer depths derived from Argo-float profile (figure not included). Bloom surface area exhibited two peaks, the secondary peak occurred on August 10th 2018, and the maximum peak occurred on September 22nd 2018 (Figure 15). The average daily CHL concentration peaked on August 30th 2018, decreased shortly thereafter and remained relatively constant for the duration of the bloom (Figure 15). The total biomass peaked on August 10th 2018, just after the bloom

reached its greatest area, and decreased at a slower rate than the chlorophyll concentration until the bloom's demise (Figure 15).

5. DISCUSSION

A. BLOOM THRESHOLD, BEHAVIOR, AND CHARACTERISTICS

Defining a bloom threshold as the median plus the MAD of the CHLA fields allows the comparison of chlorophyll blooms in locations with different background chlorophyll signals, and across a time period with large scale bloom events (outliers). This approach differs from the use of a fixed CHL bloom threshold of 0.15 mg m^{-3} as in Wilson et al. (2003), and is most similar to the mean plus the standard deviation of the monthly seasonally filtered CHL field employed by Fong et al. (2008) and Guo (2019). The purpose of the seasonal filter is to mitigate the effects of a positive chlorophyll gradient with increasing latitude in the NPSG, and to remove the photoacclimation temporal signal (Figure 2). Ultimately, we use the median monthly average over the mean monthly average as the seasonal trend, and remove the climate signal using a running window polynomial. Lastly, the bloom threshold level is less influenced by outliers when using the median plus the MAD of the CHLA fields compared to the mean plus the standard deviation of the filtered CHLA fields.

Past studies of bloom phylogeny in the NEPSG have largely excluded the Station ALOHA blooms and focused on the 30°N region (Wilson 2003, 2008, Villareal 2011, Wilson 2011, 2013). This is likely because Station ALOHA blooms do not regularly exceed the canonical 0.15 mg m^{-3} CHL threshold, even though they occur at a similar area and with similar timing. Although the absolute magnitude of phytoplankton blooms at Station ALOHA is lower than that of the 30°N blooms, the relative magnitude of

phytoplankton blooms found through analyzing climatologically filtered CHL products are similar, and of equal interest for the purpose of this study. It is likely that the physical dynamics driving the blooms at 30°N, at Station ALOHA, and between the two regions are one and the same.

While mesoscale blooms the size of Hawai'i occur every year, blooms larger than $10,000\times10^5$ km^2 occur semi-annually. These blooms tend to last approximately 30-130 days. A few blooms (2007, 2015, 2020) begin in the late summer, August - September, but persist until the winter, when they are engulfed by the subtropical chlorophyll front, making a true end date difficult to distinguish. Conversely, some blooms, notably 2005 and 2019 (see Toyoda & Okamoto 2017), begin as the subtropical chlorophyll front recedes. In some cases, 2007 and 2020, multiple large blooms occur in a single year. There was no apparent long-term trend in the start and end dates of the blooms. It is possible that there is a 4- to 5-year periodicity in the start and end dates, but does not coincide with the ENSO cycle (not shown) (Figure 3). While there is variation in the magnitude of blooms over time, there is no general increasing or decreasing trend. From 2017-2020 there were four consecutive blooms with large areas relative to past years (Table 1, Figure 4).

SUB- AND MESO-SCALE FEATURE IDENTIFICATION AND ASSOCIATION WITH PHYTOPLANKTON BLOOMS

By determining the spatial association of CHLA to meso-submesoscale features we address some of the leading hypotheses of chlorophyll bloom drivers in the NEPSG. If these interannual chlorophyll blooms are caused by the aggregation of buoyant phytoplankton, then there should be a strong association of CHLA to meso-submesoscale physical features, such as the cores of eddies or the eddy edges. If either internal

breaking waves or a convergent geostrophic flow drives the inter annual chlorophyll signal, then the CHLA will be associated with submesoscale features. If the positive CHLA values are associated with positive mesoscale features (anticyclonic-downwelling), then it is possible that buoyant nitrogen-fixing bacteria, such as *Trichodesmium*, are driving the increased CHLA satellite signal. Finally, if algal mat vertical migration causes time-delayed CHLA, then little association with submesoscale features will be found.

The cluster analysis alone cannot decouple simultaneous submesoscale productivity drivers, but can both quantify the total submesoscale contributions to CHLA, and decouple submesoscale driven CHLA from those not spatially associated with any submesoscale feature. Furthermore, it is likely that regardless of the bloom drivers, plankton will be associated with frontal features, because by definition plankton are subject to the motion of the ocean currents. This means our analysis does not provide a counterexample for the frontal "sweeping" and plankton aggregation hypothesis.

Summer blooms at Station ALOHA and those near 30°N appear to consist of similar phytoplankton, but given the proximity of Station ALOHA to the Hawaiian island archipelago, and its greater distance from the subtropical front, it is possible that the physical factors driving CHL signal at Station ALOHA differ from those driving the CHL signal in the upper NEPSG. The northern region of the study area is greatly influenced by the subtropical front that ebbs and flows with the season. The interaction of which was explored in Toyoda & Okamoto (2017). The southern region is under greater influence of surface currents generated by the Hawaiian Lee Current and North Hawaiian Ridge Current interaction with the Hawaiian ridge, producing a mass island effect that can extend further from the coast than would be expected (Gilmartin & Revelante 1974).

Lastly, baroclinic instabilities generated by the tide passing over the Hawaiian ridge induce mixing as far north as 30°N and to the south near Station ALOHA (Rudnick et al. 2003).

It is interesting to note the spatial distribution of these chlorophyll blooms has been used to study the effects that the internal breaking waves in this region have on mixing (Wilson 2011). That is, we first assume these annual phytoplankton blooms are initiated by nutrients supplied to the photic zone from internal breaking waves, then use the bloom locations and patchiness to deduce information about the physical dynamics in the region. Through this method, and given the spatial distribution of blooms characterized in this study (Figure 1, 5, 6), we could infer that baroclinic mixing occurs not only along the critical 30°N line, but also further south near Station ALOHA and the main Hawaiian Islands. This is further enforced by the five blooms that occurred across the entire study region (2006, 2014, 2015, 2018, 2020). Similarly, the spatial distribution of blooms along the 30°N line gives further evidence that the southern extent of the subtropical front is partially dictated by baroclinic waves in the NEPSG (MacKinnon & Winters 2005).

The methods outlined by Guo et al. (2019) illustrate two methods of defining submesoscale regions using SLA and FSLE fields: a threshold method and a k-means clustering method. The former utilizes the mean and standard deviation of the SLA and the FSLE, as well as the average eddy amplitude derived from eddy tracking data (Eddy Ocean Atlas) to define classification boundaries in FSLE-SLA space. We updated an approach outlined by Gou et al. (2019) where the SLA and FSLE data points are grouped into one of four physical regions based on the Euclidean distance to a centroids location

in FSLE-SLA space (Figure 7) i.e. positive mesoscale, negative mesoscale, sub-mesoscale and mixed.

We deviate from the Gou et al. (2019) method by combining the threshold method and cluster method. That is, we set the centers of the clusters to be the first and second moments of the SLA and FSLE distributions, and because the locations of those centers do not change, a Voronoi Diagram is produced (Figure 7). Furthermore, by grouping the points in this way, we simplify the k-means cluster algorithm into a Voronoi decomposition. The points are grouped based on their shortest Euclidean distance to a central location, without the iterations that occur in a traditional k-means cluster algorithm. The Guo et al. (2019) threshold method uses the average eddy amplitude to define the mesoscale positive and negative boundaries. Meaning it is an algorithm that identifies eddies and fronts, that relies on another algorithm, the py-eddy-tracker algorithm (Mason et al. 2014), that identifies eddies. Here, by only relying on the first and second moments of the FSLE and SLA fields, an independent method of identifying eddies is produced.

When indirectly comparing the positive and negative mesoscale features identified using the Veroni cluster method (Figure 7) to the outer eddy contours provided by the mesoscale eddy trajectory atlas product (METAP) (Figure 8, 9), it can be seen that the cluster method smaller and less uniform eddy areas. In this study we don't do any formal comparison of the METAP eddy realizations with eddies identified using the cluster method. With that, it is possible eddies identified here are not associated with vorticity and mixing. To address this, we use the mean plus two standard deviations of the FSLE and SLA sets, as oppose to one standard suggested in Guo et al. (2019). In this way, we select for strong eddies and fronts that are more likely to incite a mixing response. We

believe these submesoscale and mesoscale features can impact mixing, predator-prey dynamics, and nutrient input into the mixed layer. Furthermore, CHL maps of the late summer phytoplankton blooms at 30°N and Station ALOHA visually appear to be associated with sub-mesoscale features (Figure 1, 6). Lastly, for the purpose of identifying possible physical drivers of blooms in these regions, we find it important to employ a method that simultaneously determines the association of CHL anomalies to both mesoscale eddy features and sub-mesoscale frontal features.

Overall, in the NEPSG there appears to be a positive association of bloom features to anticyclonic eddies, a negative association with cyclonic eddies, and a positive association with frontal features with no apparent association with mixed regions (Figure 7). Importantly, while these are the overarching trends, there are still years where the inverse is true. Meaning there is a correlation to submesoscale features within years and across years at NEPSG. This mixed effect of SLA and FSLE on CHLA is particularly visible in the contour plot of CHLA mapped to SLA and FSLE (Figure 7). This is contrary to the findings of Guo et al. (2019), where CHLA was linearly associated with SLA and FSLE within the western region of the North Pacific Subtropical Gyre. It is unlikely then, that the blooms within the NEPSG are driven by one predominant factor, but rather a conglomerate of drivers whose components change from year to year, which is to be expected as there are multiple means to introduce nutrients and to alter predator-prey dynamics. Overall the association of anticyclonic features to bloom values was weak, and the association to cyclonic mesoscale features was negative. With this, we don't believe mesoscale eddy interactions play a major role in these large-scale phytoplankton bloom events.

While we don't find evidence to support the hypothesis that mesoscale eddy interactions are primary drivers of these blooms, we unfortunately do not resolve the true effects of submesoscale features on phytoplankton growth. Interesting submesoscale interactions occur to the sides of frontal features. That is, there is a side associated with upwelling (positive SLA) and a side associated with downwelling (negative SLA). Here we only identify the sliver where fronts occur, that separates the upwelling from downwelling regions. This is possibly why we found only a slight positive association of frontal features on CHLA, because the true interaction more nuanced. Later, in the conclusion, we suggest a method that could address this problem.

There is a correlation between CHLA and positive mesoscale features within the NEPSG for the years 2005, 2006, 2010, 2013, 2017, 2018, and 2020. This is consistent with the hypothesis that CHL anomalies are driven by the downwelling of nutrients within anticyclonic eddy cores creating nitrogen deplete surface water and generating a bloom of buoyant nitrogen-fixing phytoplankton. There is a positive correlation between CHL anomalies and negative mesoscale features for the years 2009, 2014, and 2015. This is consistent with the hypothesis that upwelling at eddy cores transports nitrogen into the surface ocean, from the nitrogen maximum below the mixed layer, which ultimately drives phytoplankton blooms. Near Station ALOHA, in the late summer of 2005, there was a positive association with positive mesoscale features. This is consistent with co-occurring shipboard observations of elevated CHL levels within an anticyclonic eddy at Station ALOHA in the late summer of 2005 (Fong et al. 2008).

While few of the blooms that occurred within the NEPSG appear to have a positive association to negative mesoscale features, the possibility that blooms are driven by

cyclonic eddy dynamics within this region cannot be ruled out. The percent associations reported in Figure 7 are bulk results, and do not account for temporal effects. The associations of each submesoscale region are time average over the lifecycle of the bloom, and it is possible that the effects of strong submesoscale associations that momentarily occur are under-reported.

Describing the association to submesoscale features in this way is useful, but it is important to note that the percent association to submesoscale features is co-variant and can provide confounding results. Meaning an increase in one association with a submesoscale region could be caused by the decrease in association with another submesoscale region, rather than being the effect of a true biophysical driver. To address this conundrum, we utilized a general additive model (GAM) that is capable of handling co-variant predictors and response variables that are spatially and temporally auto-correlated. The latter is important because we are similarly interested in the time-resolved association of CHLA to submesoscale regions from the onset to the demise of the late-summer blooms. Unfortunately, the application of a GAM to each bloom that occurred between 2002 through 2021 within the NEPG is computationally costly. We performed a case study for the 2018 bloom, with the expectation that what we find with this analysis can be extended to other blooms in the region.

B. 2018 CASE STUDY

The phenology of the 2018 bloom cannot be discussed without mention of the coincident eruption of Mt. Kilauea. Near shore volcanic drivers of phytoplankton growth have been explored and include input of nutrients into the surface ocean from direct lava

contact, and the heating of deep-water causing upwelling that supplies nitrate to the surface ocean (Wilson et al. 2019). Given that the 2018 bloom, being one of the largest in the satellite record, coincided with one of the largest volcanic eruptions in recorded history, it's possible there was some connection between the two. It would be interesting to know if the nearshore drivers volcanic of phytoplankton blooms are the same for the majority of the bloom that occurred out at sea. Unfortunately, we leave this as a curiosity and move to discussing the effects of mesoscale and submesoscale features on phytoplankton growth.

For most SLA values associated with eddy events across the 2018 bloom's lifespan, the results of the GAM negate the general belief that cyclones act as fertilization features, where cyclones increase the inventory of nutrients in the euphotic zone, and anticyclones decrease the inventory of nutrients in the euphotic zone. It does give some evidence that anticyclonic features drive increased phytoplankton abundance. This could be explained by some combination of three different effects anticyclonic features have on phytoplankton. Those are, (i) anticyclones act as anti-fertilization features allowing nitrogen fixing phytoplankton to thrive, (ii) in the northern hemisphere anticyclonic features are associated with convergent surface currents that can act to aggregate buoyant phytoplankton, and (iii) submesoscale fronts induce upwelling on their anticyclonic (positive SLA) side, meaning the positive mesoscale signal could be driven by submesoscale effects.

Contrary to the findings of past studies, we find a direct relationship between chlorophyll and SLA. Such that negative SLA, typically associated with cyclonic features, has a negative effect on CHL (Figure 11). This is further evidence that cyclonic features

drive changes at depth (below detection by satellites) while positive SLA features drive increases in chlorophyll in the near-surface waters through the accumulation of particles. This could indicate that the more non-traditional view of eddy-plankton dynamics holds for strong anticyclonic given by the three effects of anticyclonic features on phytoplankton growth listed above.

As for SLA's effect on SSTA we found a similar near-linear relationship. The negative effect of negative SLA on SSTA is evidence of cold core cyclonic eddies, and upwelling (Figure 11).   The variable effect of positive SLA on SSTA is indicative of horizontal transport by anticyclonic eddies. This is because the effect of anticyclonic eddies is dependent on the water mass where the eddy originated compared to its current location. Even with evidence of cyclonic eddies inducing upwelling, there was a negative effect of cyclonic eddies on CHLA. We present this is as further evidence mesoscale cyclonic eddy interactions (upwelling) are not responsible for driving these phytoplankton blooms.

Frontal features that are associated with positive SLA are thought to upwell nutrients into the euphotic zone, ultimately driving phytoplankton growth (Flierl & McGillicuddy 2002, Liu 2016, Hernández-Hernández et al. 2020). With this analysis, we do not distinguish between fronts associated with positive and negative SLA features. Because of this, we cannot distinguish between fronts that physically accumulate biomass, and those that stimulate new phytoplankton growth through nutrient seeding into the euphotic zone. With this, the effects of FSLE on CHL do give some evidence that phytoplankton "sweeping" is occurring within the study region, and throughout the lifespan of the 2018 bloom. Lower values of FSLE have a negative effect on CHL, and higher

values of FSLE have a positive effect on CHL (Figure 11). As high values of FSLE are associated with frontal features, it follows that there exist lower concentrations of CHL immediately outside of the frontal regions, suggesting phytoplankton biomass was "swept" into the fronts, and removed from the surrounding waters. This is not a counter-example to fronts stimulating new phytoplankton growth. It is possible for fronts to both seed nutrients into the euphotic zone, and accumulate biomass through a sweeping effect. The GAM approach alone does not decouple these effects.

Fronts identified from FSLE are not implicitly associated with vertical mixing. They are derived from geostrophic flow fields, that are derived from surface wind measurements. To show evidence that frontogenesis is in fact inducing either vertical or horizontal mixing, a map of SSTA and CHLA is shown (Figure 13). It can be seen that fronts in SSTA are associated with fronts in CHLA. We provide this as evidence that frontal mixing is occurring and injecting nutrients into the surface ocean. Furthermore, the SSTA fronts associated with mixing events, are also associated with increased CHL signal. Still, the entire extent of the 2018 bloom is not directly associated with these SSTA frontal features, and another mechanism needs must be at play to sustain the extensive area and timespan of the 2018 bloom. For that we turn to the results of the dispersion-delusion timeseries analysis.

In Lehahn et al. (Lehahn et al. 2017), the authors first suppose frontal features are seeding nutrients into the surface ocean, and initiating a bloom at the source. They then propose a "trophic cascade" that could explain how these small and short injections of nutrients into the surface ocean could sustain blooms of the sized observed within the NEPSG by altering predator-prey encounter rates. Lastly, they show evidence that this

trophic interaction is in fact occurring through a timeseries analysis on the 2007 bloom. Here we perform the same timeseries analysis, and similarly show evidence that this ecological interaction may act to sustaining the 2018 bloom beyond the frontal regions where nutrient is first injected. They propose that is the dispersion of plankton and nutrients by surface currents that drives phytoplankton dilution, which in turn reduces grazing and allows phytoplankton to thrive maintaining increased CHL satellite signal.

The average daily CHL concentration peaked on August 30th 2018, decreased shortly thereafter and remained relatively constant for the duration of the bloom (Figure 15). The total biomass peaked on August 10th 2018, just after the bloom reached its greatest area, and decreased at a slower rate than the chlorophyll concentration until the bloom's demise (Figure 15). This is consistent with Lehahn's analysis of the 2007 bloom in the region (Lehahn et al. 2017). That is, while the 2018 bloom is dispersed i.e. the area continues to increase, the average CHL concentration and bloom biomass remain relatively constant (Lehahn et al. 2017).

6. CONCLUSIONS

We observe large phytoplankton blooms that span thousands of square kilometers, and occur annually in the satellite record. While they have been deemed late summer blooms, we found these blooms begin as early as June and exist as late as November, with no apparent climatological trend in their start and end dates (Figure 3). The affirmation that these blooms are annual is important. Many papers have summarized a handful of blooms at once, but here we characterize blooms from all 23 years of the available CHL dataset, providing complete summary statistic in one source. When characterizing these blooms in the NEPSG gyre, we find it imperative to use seasonal

and climatologically filtered CHL products. Defining a bloom threshold using a method similar to the heat wave index is useful when comparing blooms at different locations and times (Hobday et al. 2016).

These large blooms occur both along the critical 30°N line of latitude as well as further south near station ALOHA and the main Hawaiian Islands. Similarly, we found blooms of similar duration, seasonal timing, patchiness, and magnitude occurred at both Station ALOHA and the 30°N critical latitude (Table 1). The bloom's magnitudes ranged from 0.22 mg m^{-3} to 0.78 mg m^{-3} with similar results for blooms near station ALOHA as those near the 30°N critical latitude. This further justifies the inclusion of Station ALOHA blooms in this analysis, and any future analysis of blooms in this region. While a few blooms appeared to branch from, or be engulfed by the subtropical chlorophyll front, many of the blooms had no apparent association with the subtropical chlorophyll front in either space or time. This indicates the blooms could be initiated by physical dynamics not wholly associated with the subtropical front, which is contrary to what previous studies suggest (Toyoda & Okamoto 2017).

We found that in general the phytoplankton blooms were associated with anticyclonic features, negatively associated with cyclonic features, and positively associated with strong frontal features (Figure 7). This gives evidence that anticyclonic features could be driving an increased chlorophyll at the surface ocean, either through the accumulation of buoyant plankton via convergent surface currents or providing a habitat for nitrogen-fixing phytoplankton to thrive. It remains possible that cyclonic eddies drive phytoplankton growth just below the surface through eddy pumping, outside the range of the satellite's optical depth. While this describes the general association of blooms in the NEPSG to

eddies and fronts, conversely there exists years where bloom features that are negatively associated to anticyclonic eddies and positively associated with cyclonic eddies. This indicates that there are likely multiple bloom drivers, whose interactions change between years.

Previous studies have stated there is either no correlation to SLA and SSTA (White et al. 2007, Dore et al. 2008) or positive correlation to cyclonic mesoscale features (Wilson 2021). We show that there is a negative association to cyclonic features both given by the bulk analysis (Figure 7), and the generalized additive model of the 2018 bloom (Figure 11). While no apparent trend between CHL, SLA and SSTA was previously found, a call for higher resolution physical datasets was made (White et al. 2007). Here, with the use of the ultra-high-resolution MUR SSTA L4 data set, we do see a relationship between SSTA fronts and CHLA fronts. Furthermore, with the use of the same MUR SSTA dataset, we present evidence that at least for the 2018 bloom, submesoscale mixing is occurring.

The 2018 bloom covered the largest area of any bloom in the NEPSG, spanned the entire study region, and began conspicuously soon after the 2018 eruption of Mount Kilauea and the formation of the Kamaʻehuakanaloa seamount. Given by the relationship of SLA, SSTA and CHLA elucidated by the generalized additive model (Figure 11), we do not believe the 2018 bloom was driven by typical cyclonic mesoscale eddy interactions. But, by comparing SSTA and CHL maps, we find an association between phytoplankton fronts, and temperature fronts. We present this as evidence that the onset of the 2018 bloom was facilitated by vertical mixing of nutrients into the euphotic zone by submesoscale features. Once the bloom was initiated by sporadic, small scale nutrient injection, we believe the temporal and spatial extent of the bloom persisted beyond the

submesoscale through the delusion-dispersion effect (Lehahn et al. 2017). Through the

comparison of bloom biomass, concentration, and area timeseries (Lehahn et al. 2017),

we show evidence that the delusion-dispersion effect did play a role in sustaining the

2018 bloom. While this does not explicitly hold for all late summer blooms within the

NEPSG, we believe the 2018 blooms story can be extended to other blooms in this region.

7. TABLES

Table 1: Summary table of late summer CHL blooms in the NPSG

Summary statistics of each bloom within the NEPSG study region between 2003 to 2021. Magnitude taken as the maximum CHL [mg m^{-3}] value the blooms reached, and area is the maximum area the bloom reached, duration as the difference between the start and end dates of the bloom. Longitude and Latitude are the bloom's center coordinates.

Start date	Duration [days]	Magnitude [mg m^{-3}]	Area [km^2 x 10^5]	Latitude	Longitude
7/29/1997	99	0.32	16.6	30.4	-146.4
7/8/1998	90	0.20	6.9	27.4	-154.3
8/1/1999	72	0.28	6.7	31.1	-137.7
8/15/2000	92	0.33	7.8	30.4	-152.9
6/15/2002	87	0.15	7.9	30.2	-145.4
7/26/2003	74	0.20	12.3	31.7	-139.6
6/3/2004	69	0.27	17.0	31.6	-141.4
7/2/2005	92	0.14	4.2	22.7	-153.6
7/22/2006	112	0.16	10.3	31.6	-152.7
8/15/2007	84	0.31	12.3	31.6	-156.1
8/10/2008	73	0.22	10.1	34.1	-153.2
6/13/2009	119	0.15	4.8	26.3	-143.6
7/1/2010	89	1.42	3.6	34.4	-130.4
9/7/2011	66	0.16	18.7	22.7	-151.3
9/1/2012	66	0.14	4.4	26.9	-156.7
7/10/2013	84	0.18	5.9	26.9	-151.8
6/14/2014	79	0.28	7.4	31.9	-137.7
8/1/2015	61	0.10	4.3	23.9	-155.8
8/2/2016	54	0.09	6.3	23.8	-148.0
7/30/2017	37	0.12	12.8	26.2	-159.6
7/16/2018	103	0.22	31.8	24.7	-149.1
6/11/2019	89	0.34	20.6	31.0	-137.9
6/1/2020	131	0.35	14.9	34.6	-153.1
8/1/2021	61	0.15	4.0	33.5	-149.7
7/1/2022	101	0.18	4.8	23.2	-153.6

Average summer chlorophyll (globcolor) anomaly from 1997-2022
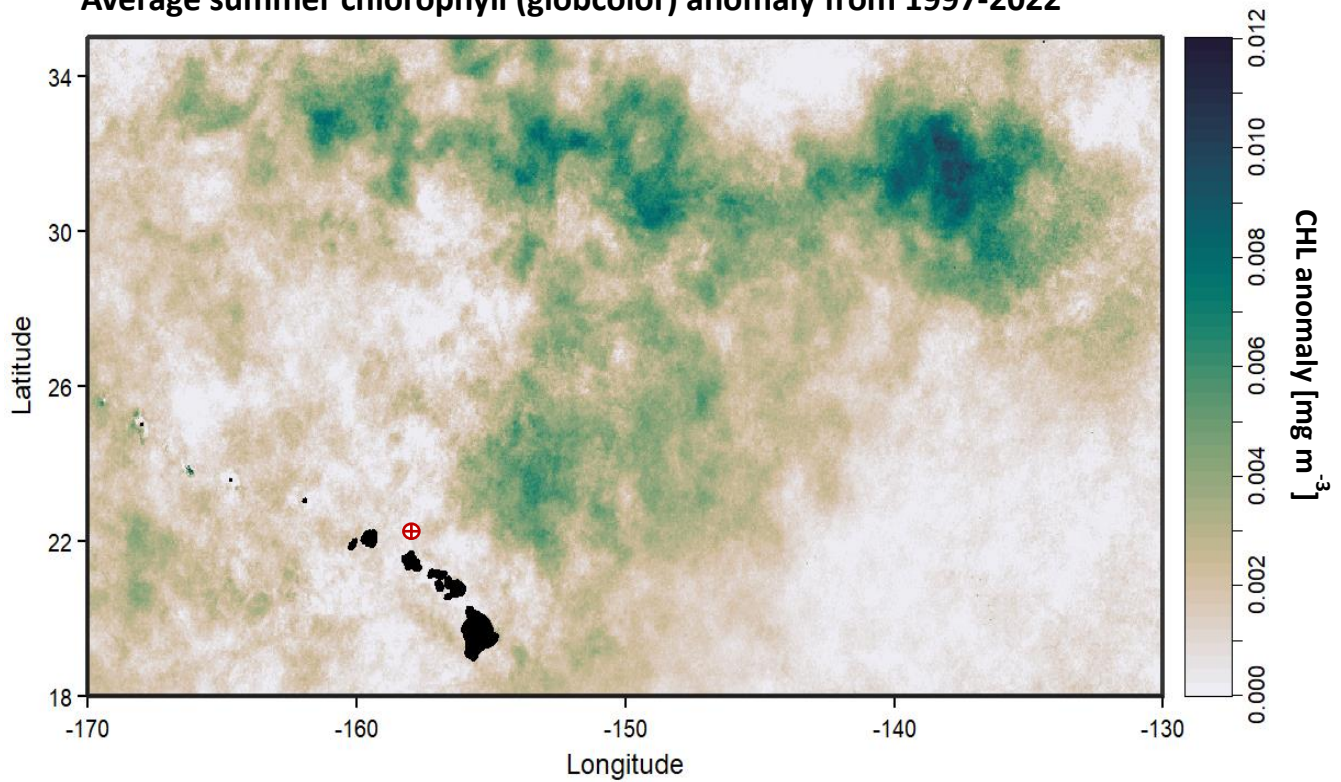
Figure 1: Contour map of the average late summer (June - October) chlorophyll anomaly, from 1997 to 2022. The map's extent is the boundaries of the study region. Hawaiian Islands are shown in the bottom left with Station ALOHA (22.75°N, 158°W) as the red dot.
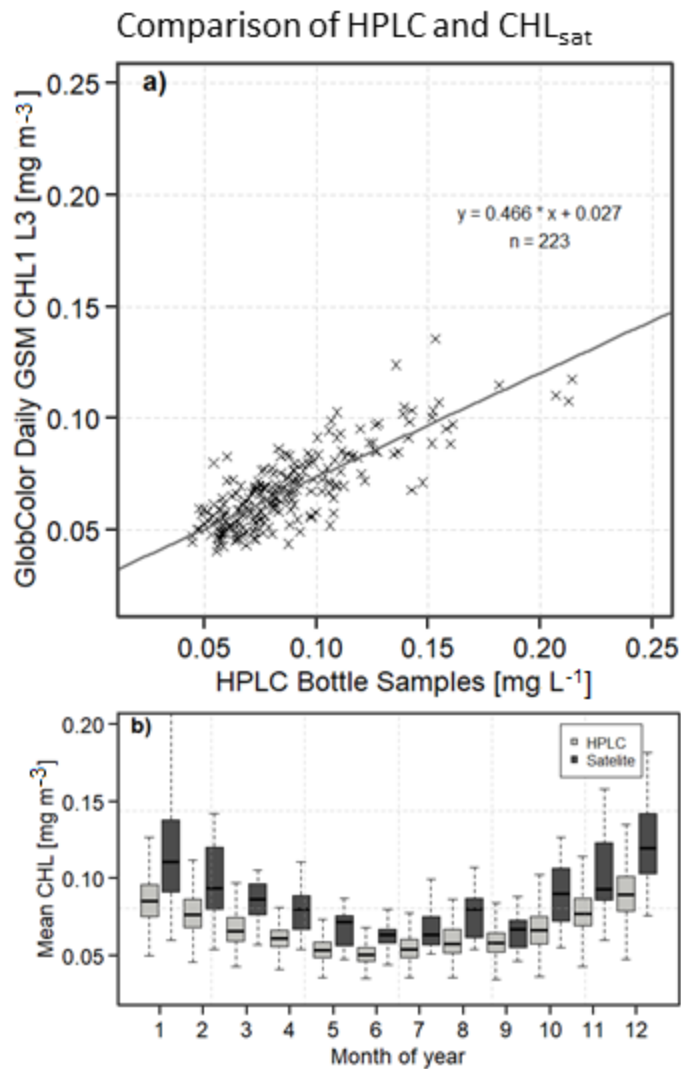
Figure 2: Comparison of High-pressure Liquid Chromatography (HPLC) bottle samples and the GlobColor CHL1 Lm3 satellite product. The satellite data is extracted from a 3x3 grid around Stn. ALOHA. HPLC bottle samples are shipboard samples taken at St. ALOHA. The generalized linear regression (family = gamma) gives an r^2 value of 0.46 with a significant fit ($p < 0.05$). Figure b) a box plot of the average monthly CHL satellite and HPLC signal across the 25 years of data (1997-2022). The light grey boxes are for the HPLC bottle samples, and the dark grey box is for the CHL satellite product.
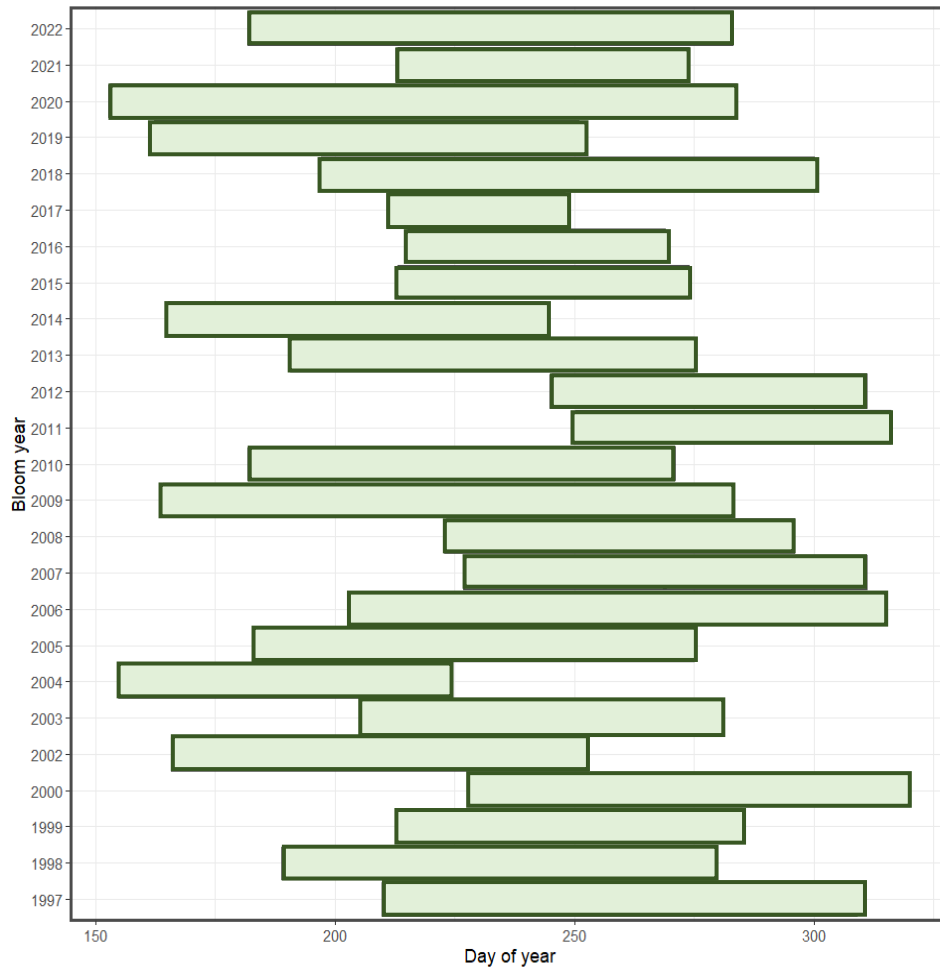
Figure 3: Durations of all phytoplankton blooms from 1997 to 2022 within the study region (18°N, 35°N, 130°W, 170°W). Horizontal length of bars indicates bloom duration and the days of the year each bloom spanned. Rows indicate the years the bloom occurred. Created by viewing weekly maps of the GlobColor CHL1 Lm3 satellite product.
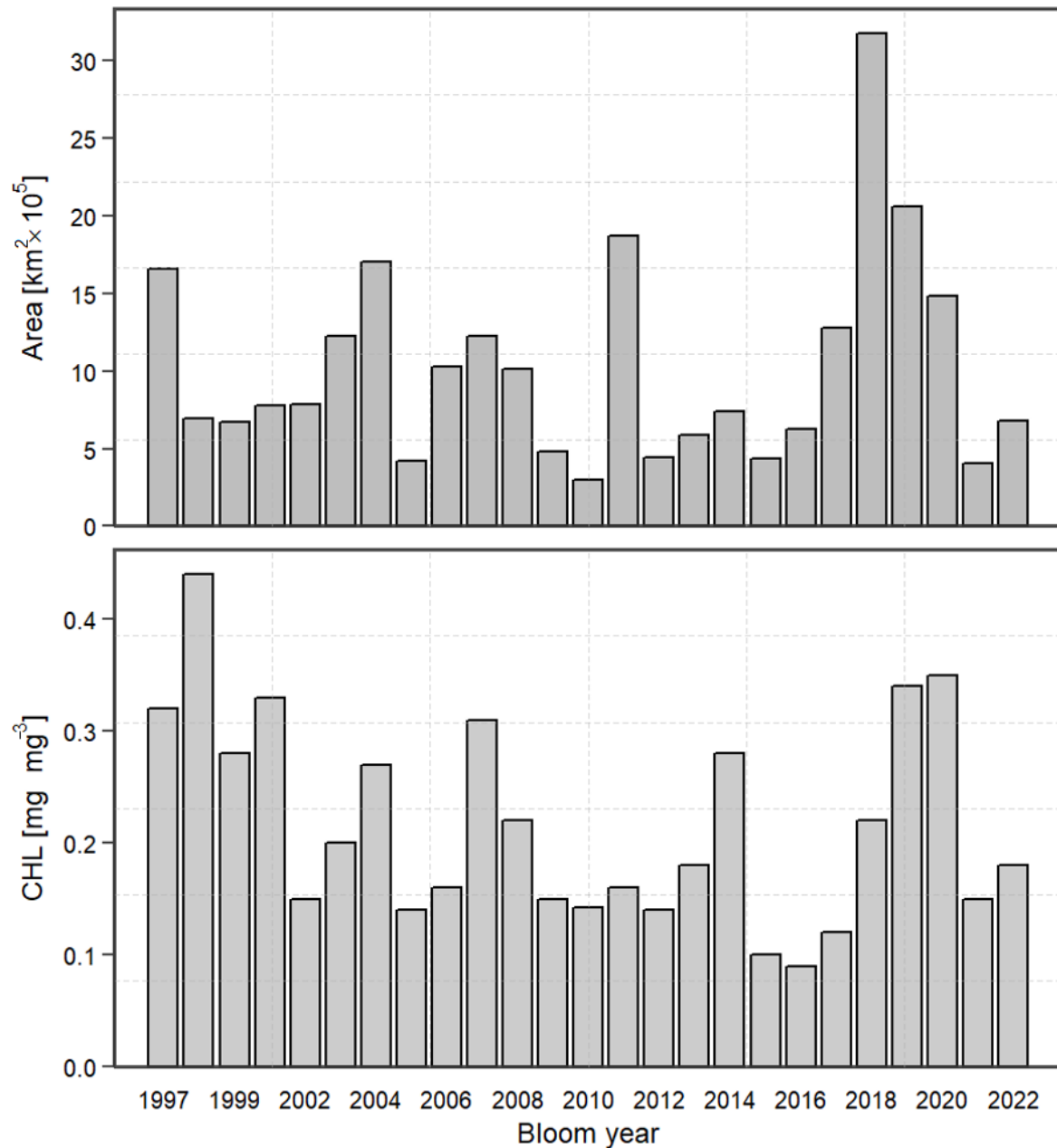
Figure 4: Bloom area (top figure) and magnitude (bottom figure) of all phytoplankton blooms from 1997 to 2022 within the study region (18°N, 35°N, 130°W, 170°W). Bloom area calculated using bloom values identified from the chlorophyll anomaly.
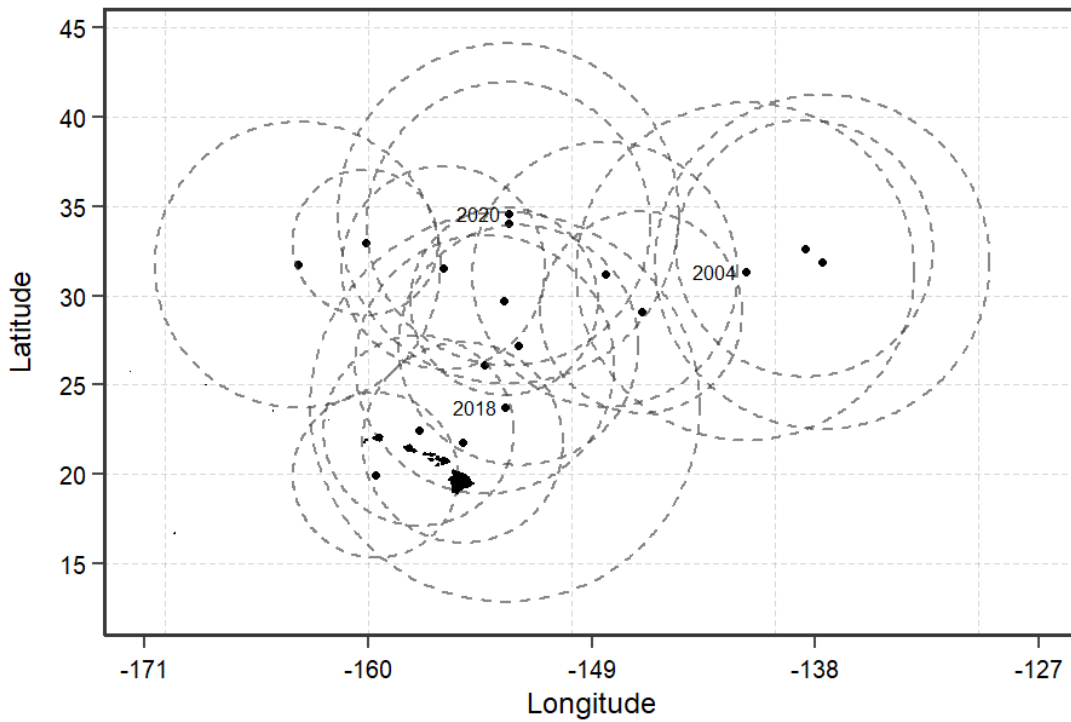
Figure 5: Bloom centers for all summer to fall blooms that occur between 2003-2020. The area of each circle is equal to the maximum area each bloom reached, calculated from the merged 8-day GlobColor CHL1 Lm3 product. Years with the largest blooms are marked with text at their centers.
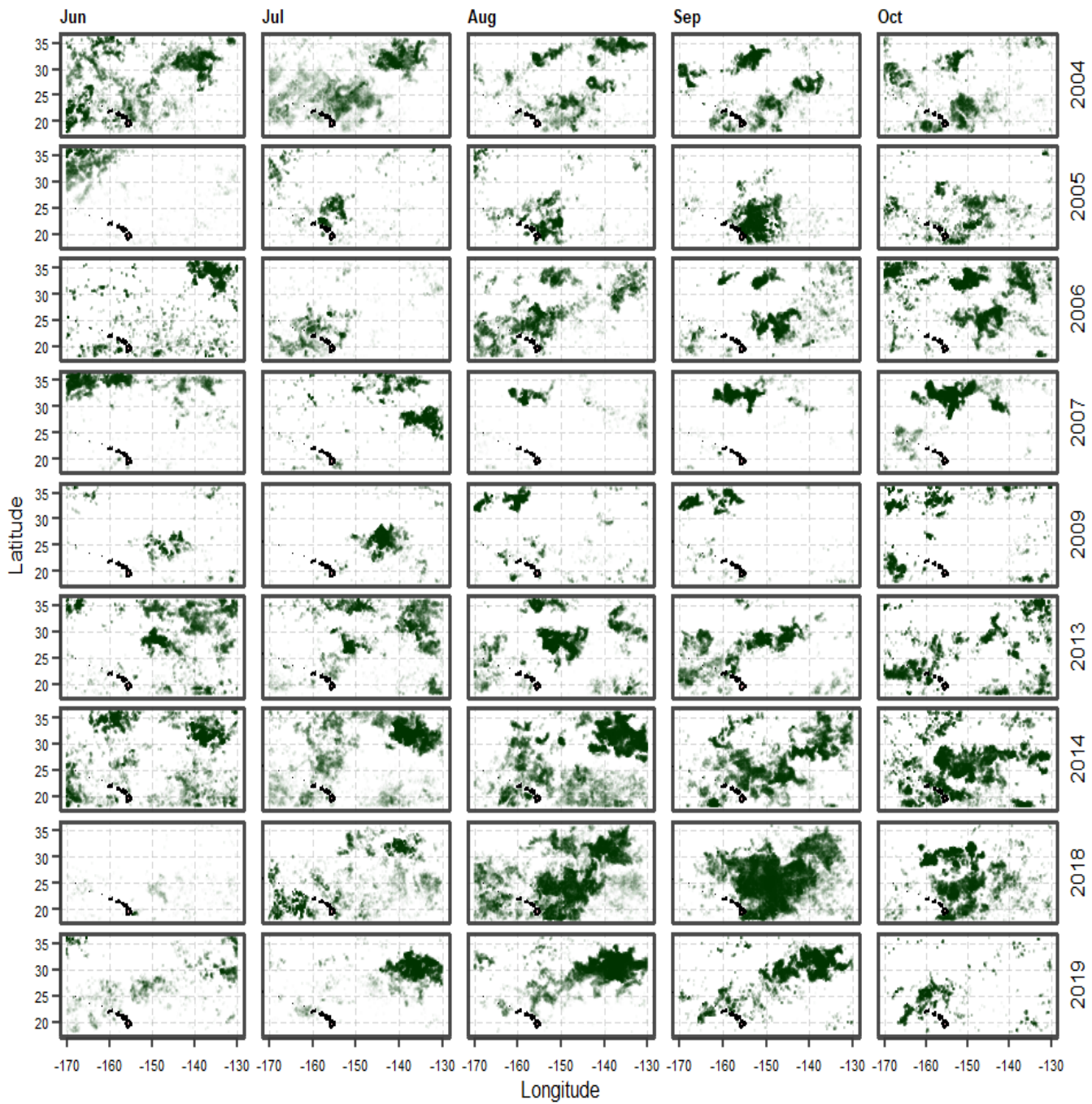
Figure 6: Monthly images of CHL bloom values within the chosen study region of the NPSG. Each row shows a unique year, and the five late summer months in which the blooms occur. The Hawaiian Islands are shown in the bottom left in black. Bloom values are found using the CHL anomaly product.
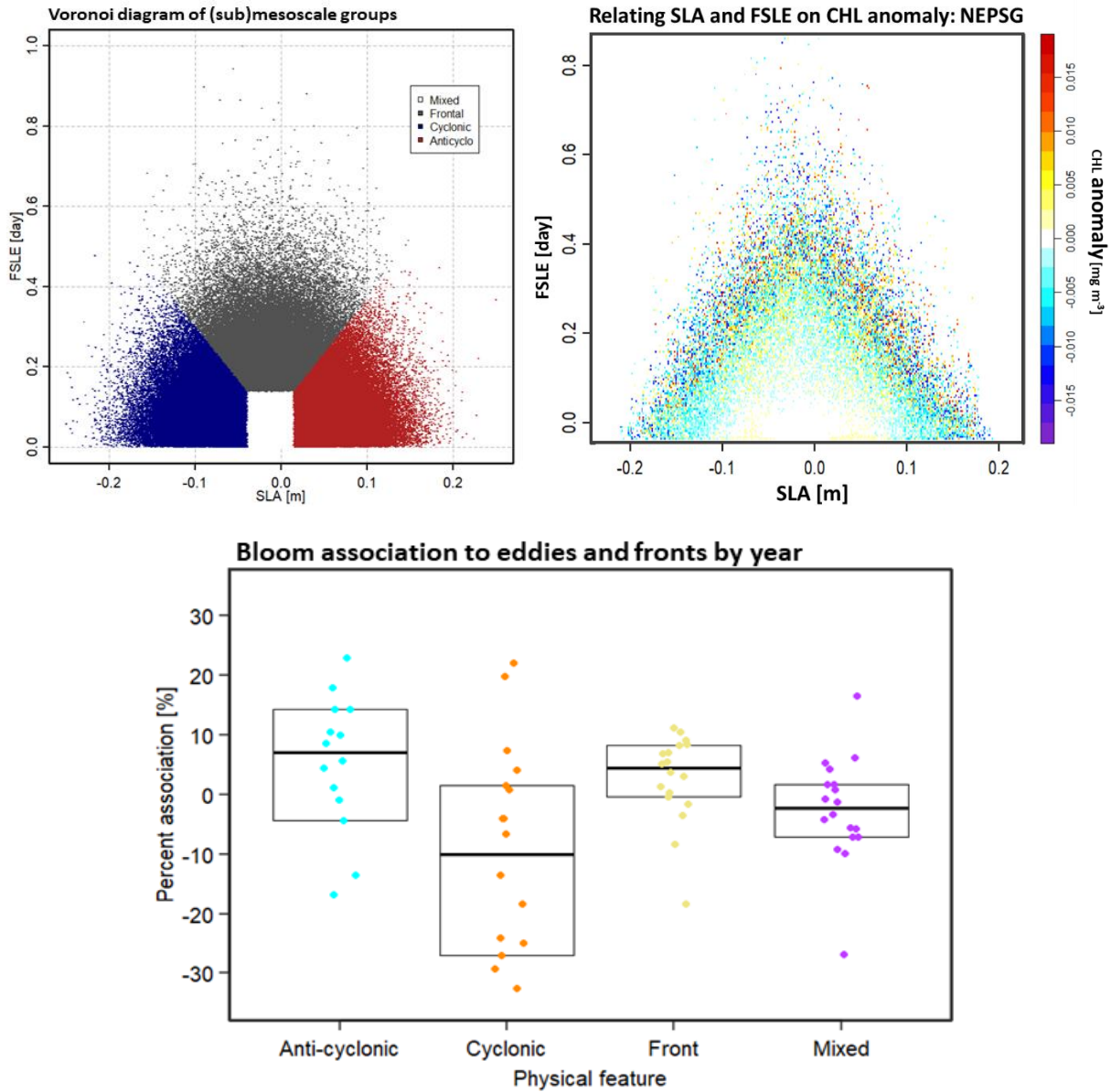
Figure 7: Veroni diagram (method: Euclidean distance, centers: 4, scaled: 0 - 1) applied to the FSLE, and SLA fields (top left figure) of a synthetic dataset displayed as a example. The Veroni decomposition groups each data point into one of four (sub)mesoscale regions: mesoscale positive (anti-cyclonic), mesoscale negative (cyclonic), submesoscale (fronts), and mixed regions. Top right figure is a contour plot of late summer CHL anomaly mapped to FSLE, and SLA fields within the NEPSG study region during the late summer months (July-October), across the entire time domain 2002-2022. The bottom figure shows the percent association of chlorophyll bloom values to (sub)mesoscale features for each late summer period, with the point in each group corresponding to a summer from a different year.
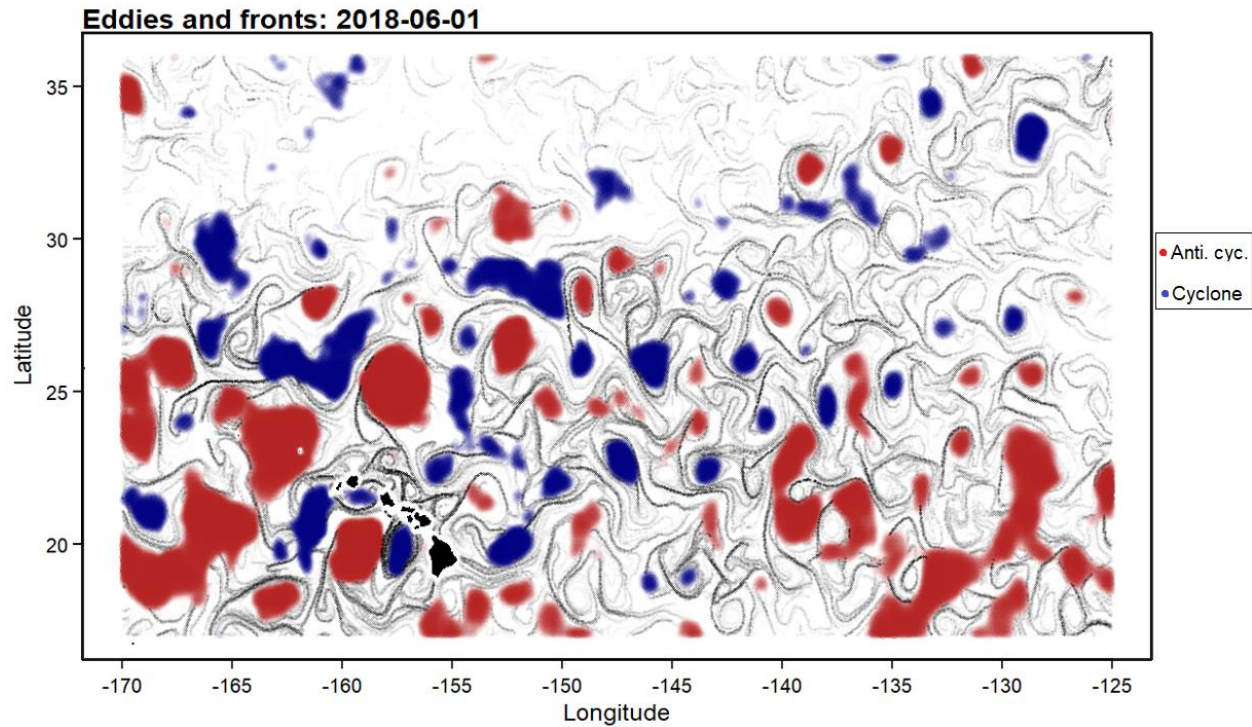
Figure 8: Re-gridded (sub)mesoscale features identified using a Veroni decomposition shown as cyclonic eddies (blue), anticyclonic eddies (red), and frontal features (dark grey). The day 2018-06-01 was randomly chosen to visualize eddies identified from SLA and FSLE.
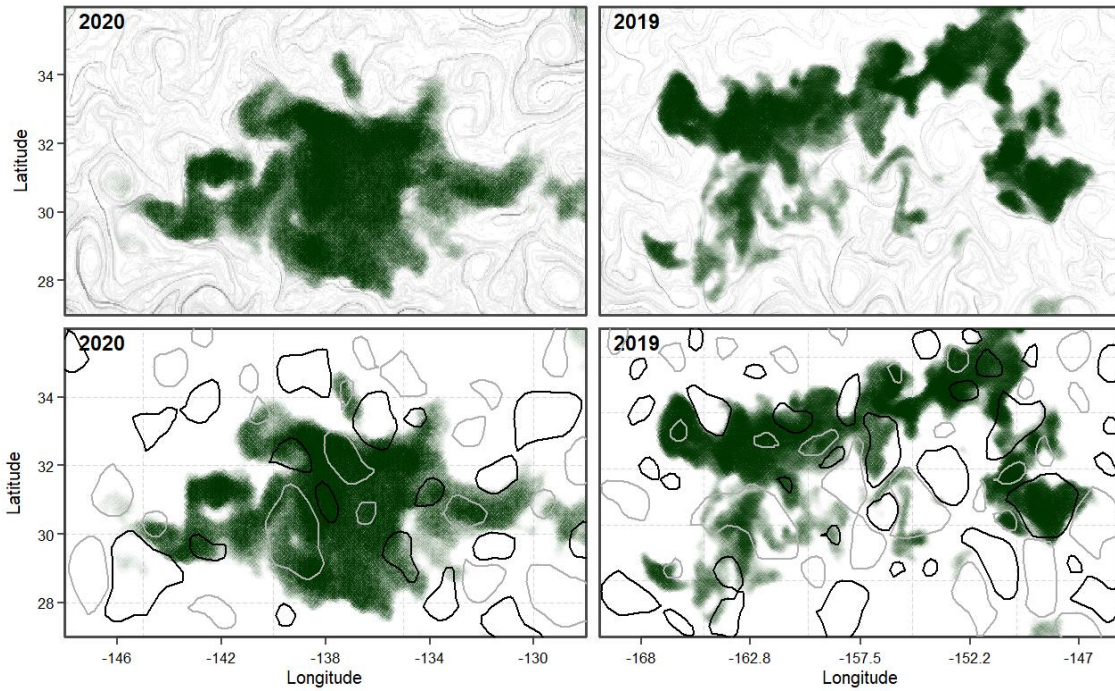
Figure 9: Plankton bloom for 2019 and 2020 overlaid by FSLE fronts (top row) and METAP eddies (bottom row). Cyclonic eddies are black polygons, anticyclonic eddies are grey polygons. Both blooms appear to be associated with frontal features with little apparent association to mesoscale eddies.
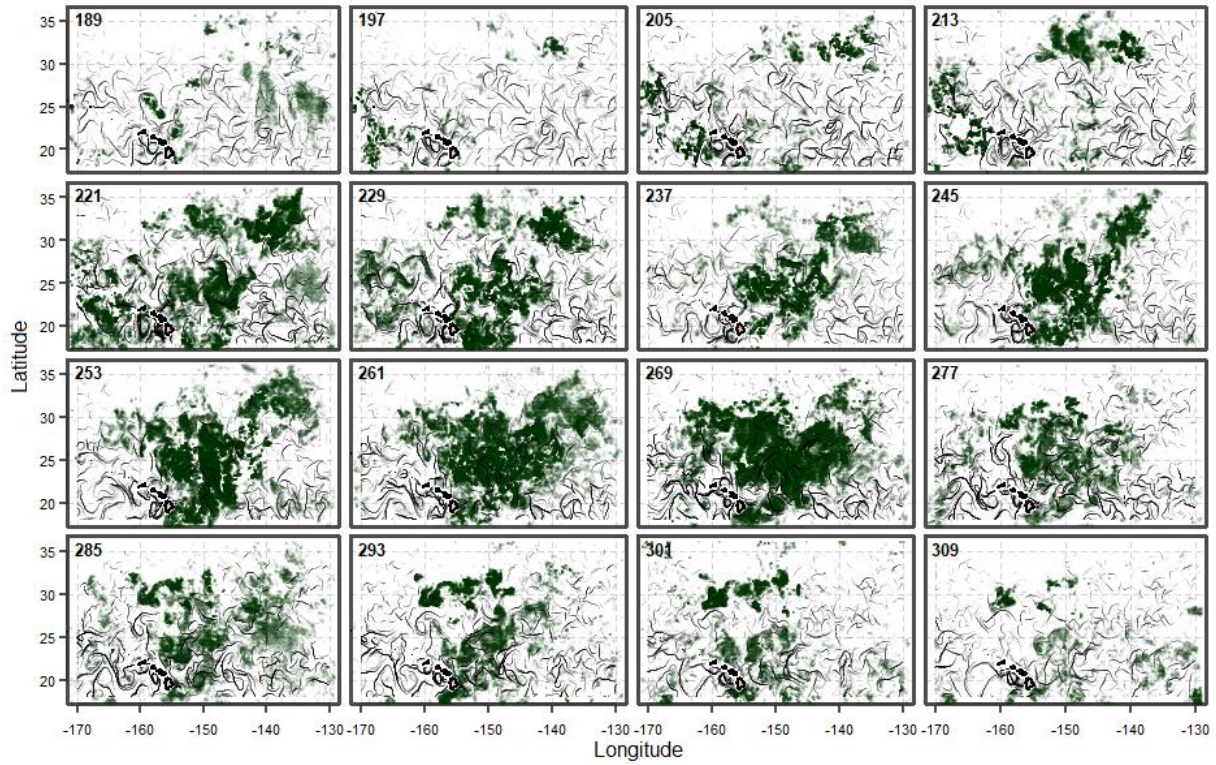
Figure 10: 8 day composites showing the start and demise of the 2018 bloom in the NSPG. Bloom values are chosen using the CHL anomaly. Strong frontal features from FSLE satellite data are shown as black lines. Day of the year is shown in the top left corner of each plot.
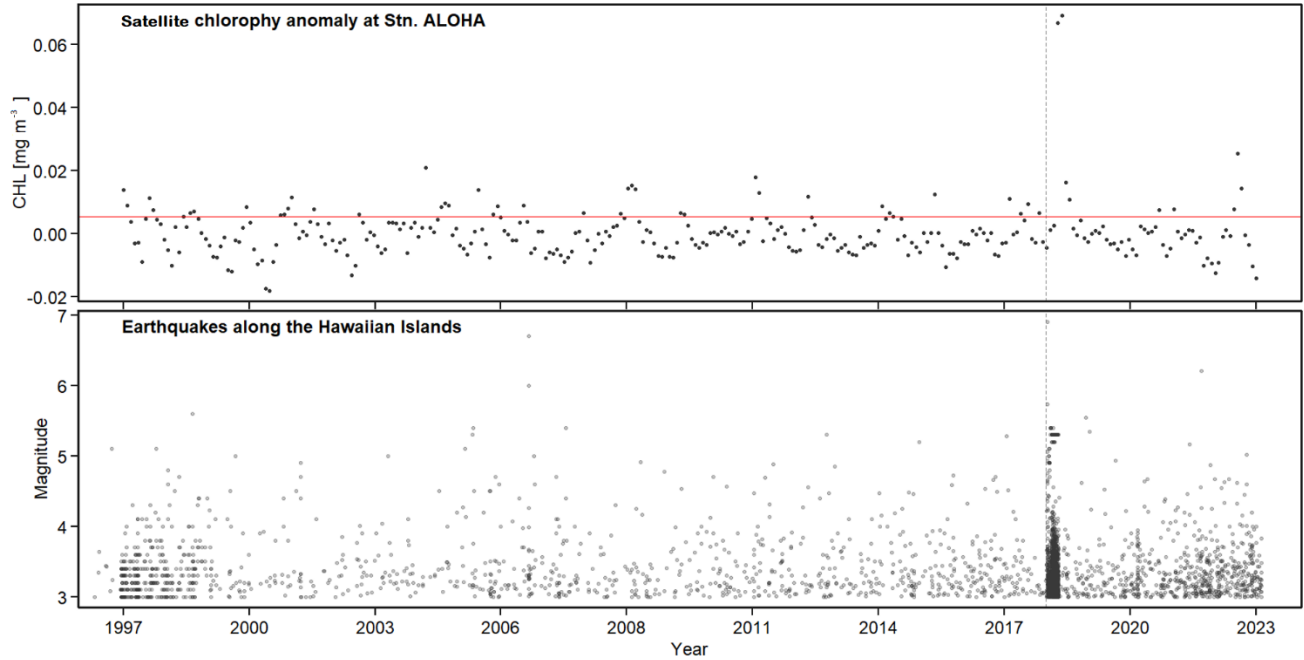
Figure 11: Top figure shows the monthly average of the GlobColor CHL1 Lm3 satellite product for a 3x3 pixel grid centered around Stn. ALOHA (22°N, 158°W), with the red line showing an example bloom threshold, and the red circle drawing attention to the 2018 bloom months. The bottom figure shows occurrences of earthquakes above magnitude 3 along the Hawaiian ridge at a daily resolution. The vertical grid dotted line denotes the beginning of the 2018 eruption and the beginning of the 2018 phytoplankton bloom.
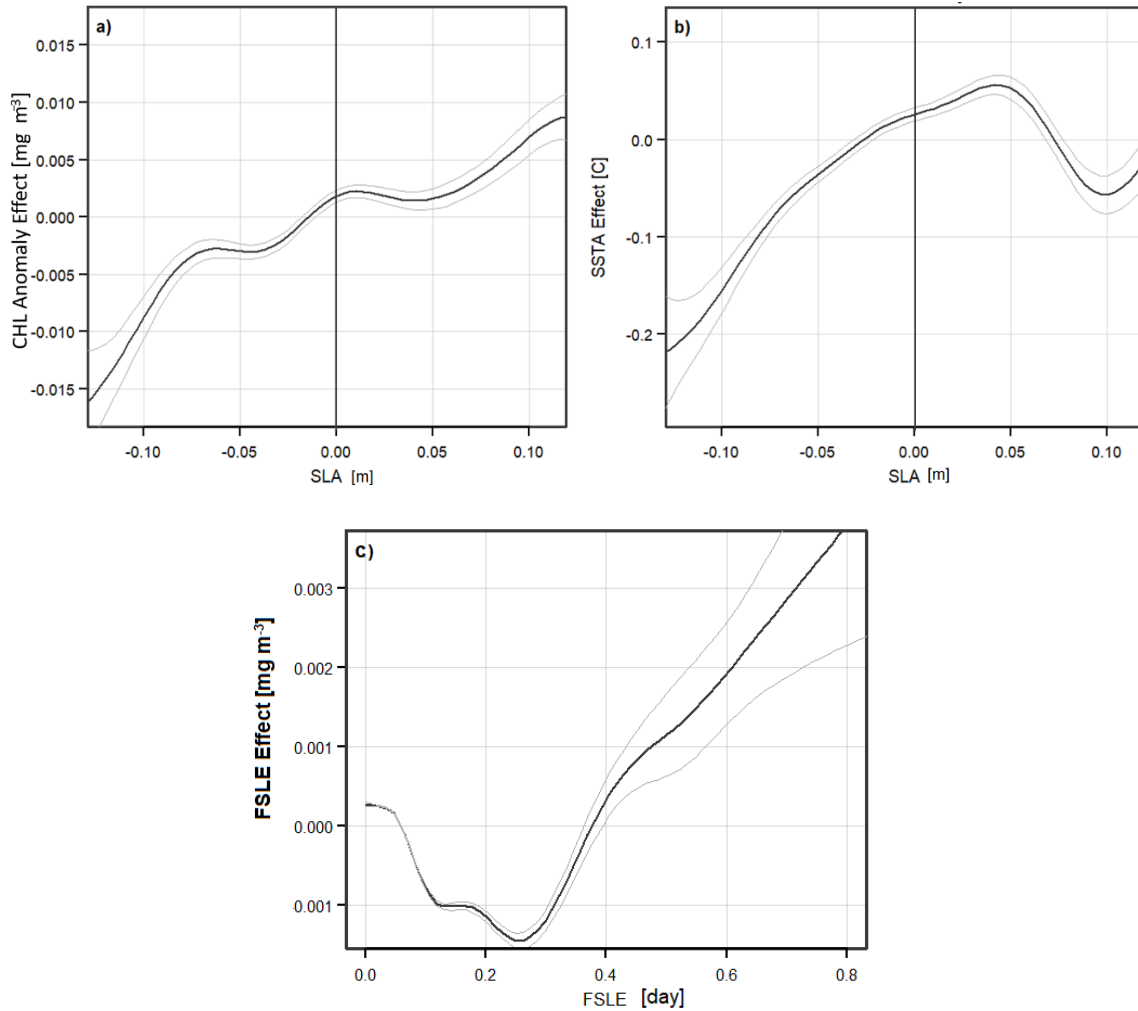
Figure 12: Generalized additive model effect results of SLA on CHL (figure a), SLA on SSTA (figure b), and FSLE on CHL (figure c). Negative SLA is used as a proxy for cyclonic eddies, positive SLA is used as a proxy for anti-cyclonic eddies, and FSLE as a proxy for frontal features. Black vertical lines (figure a. and b.) denote the zero value of SLA that loosely separates anticyclonic eddy and cyclonic eddy regions.
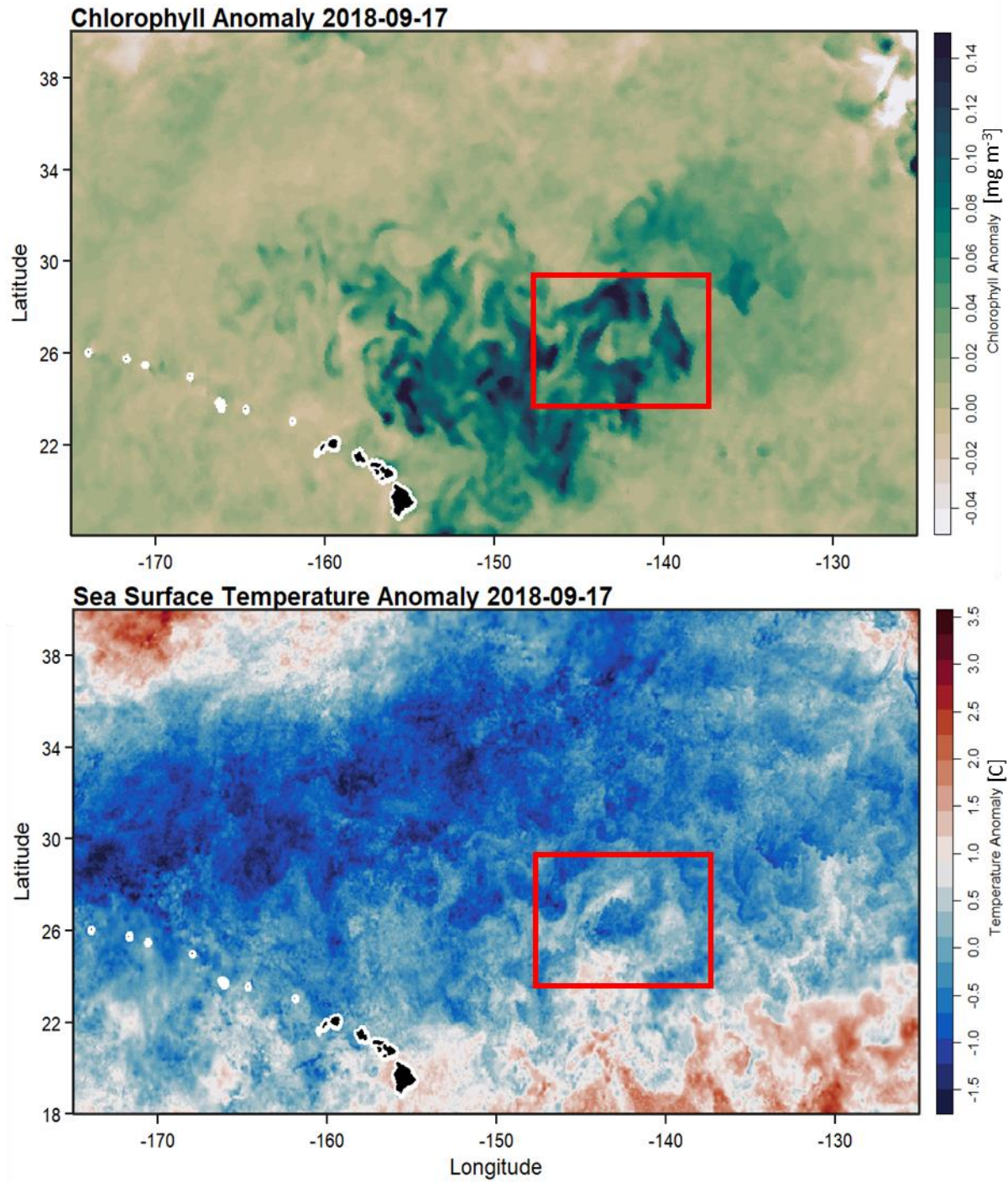
Figure 13: Map of GlobColor CHL1 Lm3 satellite product, and the GHRSST level 4 MUR SSTA satellite product for the day 2018-09-17. The purpose of the red box is to draw attention to a region, amongst others, where there is clear association between temperature fronts and chlorophyll fronts.
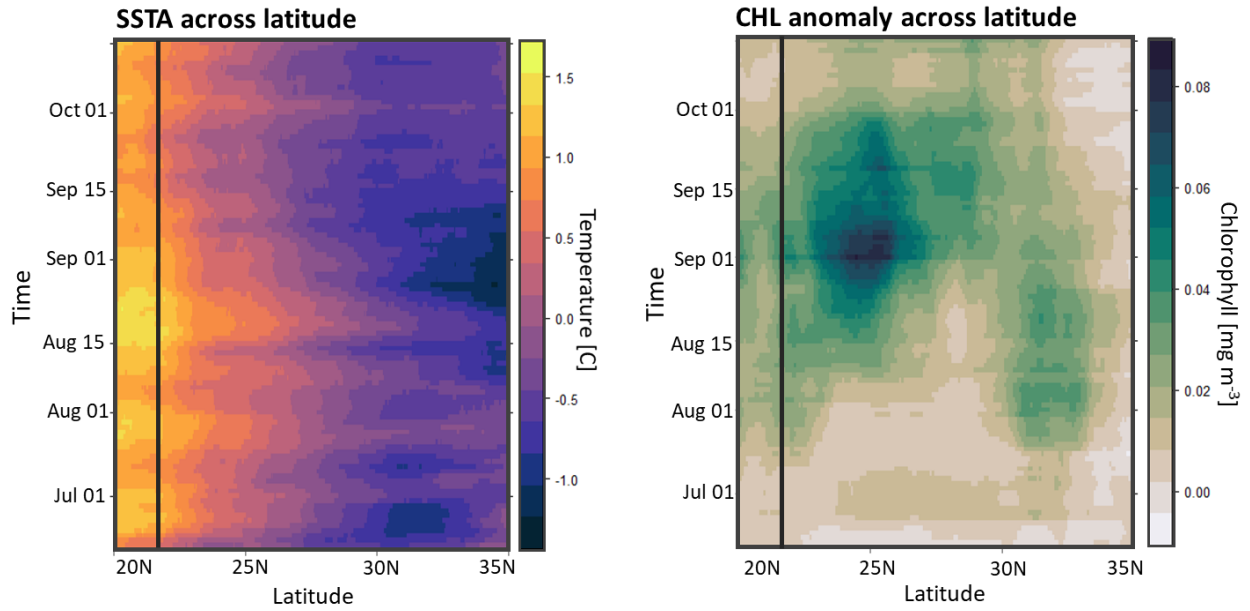
Figure 14: Hovmöller plots of the GlobColor CHL1 Lm3 satellite product, and the GHRSST level 4 MUR SSTA satellite product for the extent (18, 35, -155, -130) and across the time span of 2018-08 to 01-2018-08. The black vertical line indicates the latitude location of Stn. ALOHA, which is also near the main Hawaiian Islands. The 2018 phytoplankton bloom began near August 1st, persisted until October 1st, and was centered around 25°N.
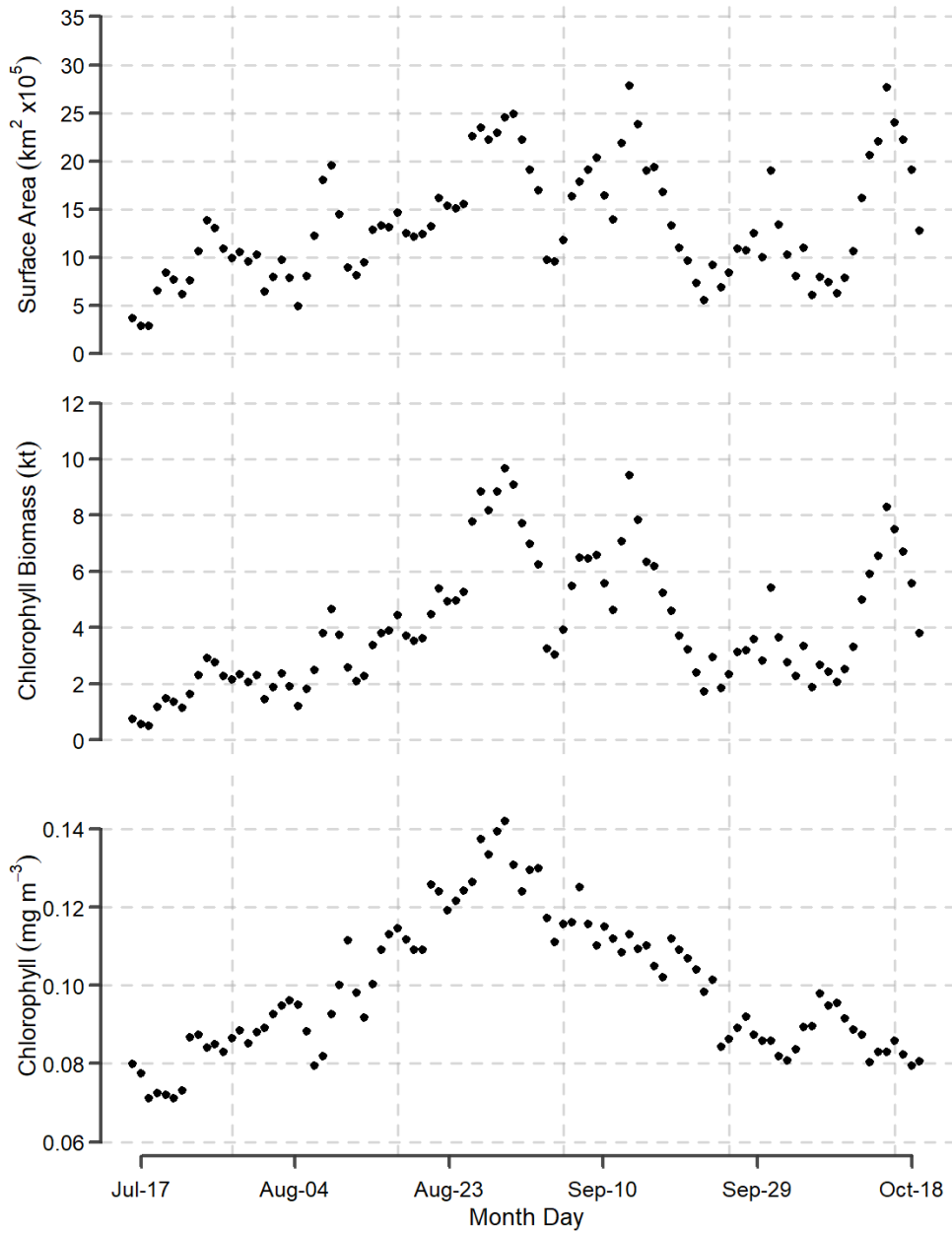
Figure 15: Timeseries progression of the onset and demise of the 2018 bloom in the NPSG. Figure a) shows the surface are, figure b) shows the biomass, and figure c) shows the CHL concentration. Mixed layer depth found using ARGO float temperature and salinity depth profiles at the bloom's location.

9. REFERENCES

Campbell L, Liu H, Nolla HA, Vaulot D (1997) Annual variability of phytoplankton and bacteria in the subtropical North Pacific Ocean at Station ALOHA during the 1991–1994 ENSO event. Deep-sea research Part I, Oceanographic research papers 44:167-192

Campbell L, Nolla H, Vaulot D (1994) The importance of Prochlorococcus to community structure in the central North Pacific Ocean. Limnology and oceanography 39:954-961

Capone DG, Subramaniam A, Montoya JP, Voss M, Humborg C, Johansen AM, Siefert RL, Carpenter EJ (1998) An extensive bloom of the N sub(2)-fixing cyanobacterium Trichodesmium erythraeum in the central Arabian Sea. Marine Ecology Progress Series [Mar Ecol Prog Ser] 172:281-292

Chu PC, Fan C (2011) Maximum angle method for determining mixed layer depth from seaglider data. Journal of oceanography 67:219-230

Church MJ, Mahaffey C, Letelier RM, Lukas R, Zehr JP, Karl DM (2009) Physical forcing of nitrogen fixation and diazotroph community structure in the North Pacific subtropical gyre. Global Biogeochemical Cycles 23

Dore J, Böttjer D, Karl D, Letelier R, Mahaffey C, Wilson S, Zehr J, Church M (2016) Temporal Variability in Nitrogen Fixation and Particulate Nitrogen Export at Station ALOHA. American Geophysical Union 2016:B34B-0350

Dore JE, Letelier RM, Church MJ, Lukas R, Karl DM (2008) Summer phytoplankton blooms in the oligotrophic North Pacific Subtropical Gyre: Historical perspective and recent observations. Progress in Oceanography 76:2-38

Flierl G, McGillicuddy DJ (2002) Mesoscale and submesoscale physical-biological interactions. The sea 12:113-185

Follett CL, White AE, Wilson ST, Follows MJ (2018) Nitrogen fixation rates diagnosed from diurnal changes in elemental stoichiometry. Limnology and Oceanography 63:1911-1923

Fong AA, Karl DM, Lukas R, Letelier RM, Zehr JP, Church MJ (2008) Nitrogen fixation in an anticyclonic eddy in the oligotrophic North Pacific Ocean. The ISME Journal 2:663-676

Friedrich T, Powell B, Stock C, Hahn-Woernle L, Dussin R, Curchitser E (2021) Drivers of Phytoplankton Blooms in Hawaii: A Regional Model Study. Journal of Geophysical Research: Oceans 126:e2020JC017069

Fu LL (2009) Pattern and velocity of propagation of the global ocean eddy variability. Journal of Geophysical Research: Oceans 114

Gilmartin M, Revelante N (1974) The 'island mass' effect on the phytoplankton and primary production of the Hawaiian Islands. Journal of Experimental Marine Biology and Ecology 16:181-204

Graff JR, Westberry TK, Milligan AJ, Brown MB, Olmo GD, Reifel KM, Behrenfeld MJ (2016) Photoacclimation of natural phytoplankton communities. Marine Ecology Progress Series 542:51-62

Guidi L, Calil PHR, Duhamel S, Björkman KM, Doney SC, Jackson GA, Li B, Church MJ, Tozzi S, Kolber ZS, Richards KJ, Fong AA, Letelier RM, Gorsky G, Stemmann L, Karl DM (2012) Does eddy-eddy interaction control surface phytoplankton distribution and carbon export in the North Pacific Subtropical Gyre? Journal of Geophysical Research: Biogeosciences 117

Gundersen K, Corbin J, Hanson C, Hanson M, Hanson R, Russell D, Stollar A, Yamada O (1976) Structure and biological dynamics of the oligotrophic ocean photic zone off the Hawaiian Islands.

Guo M, et al. (2019) Mesoscale and Submesoscale Contributions to High Sea Surface Chlorophyll in Subtropical Gyres. Geophysical Research Letters 46:13217 - 13226

Hernández-Carrasco I, et al. (2011) How Reliable Are Finite-Size Lyapunov Exponents for the Assessment of Ocean Dynamics? Ocean Modelling 36:208–218

Hernández-Hernández N, Arístegui J, Montero MF, Velasco-Senovilla E, Baltar F, Marrero-Díaz Á, Martínez-Marrero A, Rodríguez-Santana Á (2020) Drivers of Plankton Distribution Across Mesoscale Eddies at Submesoscale Range. Frontiers in Marine Science 7

Hobday AJ, Alexander LV, Perkins SE, Smale DA, Straub SC, Oliver ECJ, Benthuysen JA, Burrows MT, Donat MG, Feng M, Holbrook NJ, Moore PJ, Scannell HA, Sen Gupta A, Wernberg T (2016) A hierarchical approach to defining marine heatwaves. Progress in Oceanography 141:227-238

Irwin AJ, Oliver MJ (2009) Are ocean deserts getting larger? Geophysical Research Letters 36

Karl DM (2002) Nutrient dynamics in the deep blue sea. TRENDS in Microbiology 10:410-418

Karl DM, Church MJ, Dore JE, Letelier RM, Mahaffey C (2012) Predictable and efficient carbon sequestration in the North Pacific Ocean supported by symbiotic nitrogen fixation. Proceedings of the National Academy of Sciences 109:1842-1849

Karl DM, Letelier RM, Bidigare RR, Björkman KM, Church MJ, Dore JE, White AE (2021) Seasonal-to-decadal scale variability in primary production and particulate matter export at Station ALOHA. Progress in Oceanography 195:102563

Klymak JM, Moum JN, Nash JD, Kunze E, Girton JB, Carter GS, Lee CM, Sanford TB, Gregg MC (2006) An estimate of tidal energy lost to turbulence at the Hawaiian Ridge. Journal of Physical Oceanography 36:1148-1164

Lehahn Y, Koren I, Sharoni S, d'Ovidio F, Vardi A, Boss E (2017) Dispersion/dilution enhances phytoplankton blooms in low-nutrient waters. Nature Communications 8:14868

Letelier RM, Karl DM (1996) Role of Trichodesmium spp. in the productivity of the subtropical North Pacific Ocean. Marine ecology progress series Oldendorf [MAR ECOL PROG SER] 133:1-3

Letelier RM, Karl DM, Abbott MR, Flament P, Freilich M, Lukas R, Strub T (2000) Role of late winter mesoscale events in the biogeochemical variability of the upper water column of the North Pacific Subtropical Gyre. Journal of Geophysical Research: Oceans 105:28723-28739

Liu X, and Naomi M. Levine (2016) Enhancement of Phytoplankton Chlorophyll by Submesoscale Frontal Dynamics in the North Pacific Subtropical Gyre. Geophysical Research Letters 43:1651 - 1659

LoCicero Ve Proceedings of the First International Conference on Toxic Dinoflagellate Blooms In.

MacKinnon J, Winters K (2005) Subtropical catastrophe: Significant loss of low-mode tidal energy at 28.9°. Geophysical Research Letters 32

Mague TH, Mague FC, Holm-Hansen O (1977) Physiology and chemical composition of nitrogen-fixing phytoplankton in the Central North Pacific Ocean. Marine Biology [Mar Biol] 41:213-227

Marumo R, Asaoka O (1974) Distribution of pelagic blue-green algae in the North Pacific Ocean. Journal of the Oceanographical Society of Japan 30:77-85

Mason E, Pascual A, McWilliams JC (2014) A new sea surface height–based code for oceanic mesoscale eddy tracking. Journal of Atmospheric and Oceanic Technology 31:1181-1188

McGillicuddy Jr D, Robinson A (1997) Eddy-induced nutrient supply and new production in the Sargasso Sea. Deep Sea Research Part I: Oceanographic Research Papers 44:1427-1450

Mohler WA (1941) [A phenomenon of blue-green algae on the beach of Balikpan]. Natuurwet Tijdschr 101:75-79

O'Reilly JE, S.B. Hooker and E.R. Firestone (2000) SeaWiFS Postlaunch Calibration and Validation Analyses. NASA Tech Memo 11

Ogniewicz RL, Kübler O (1995) Hierarchic Voronoi skeletons. Pattern Recognition 28:343-359

Rudnick DL, Boyd TJ, Brainard RE, Carter GS, Egbert GD, Gregg MC, Holloway PE, Klymak JM, Kunze E, Lee CM (2003) From tides to mixing along the Hawaiian Ridge. science 301:355-357

Siswanto E, et al. (2016) Sixteen-Year Phytoplankton Biomass Trends in the Northwestern Pacific Ocean Observed by the SeaWiFS and MODIS Ocean Color Sensors. . Journal of Oceanography 72:479 - 489

Smayda TJ (1997) What is a bloom? A commentary. Limnology and Oceanography 42:1132-1136

Sverdrup H (1953) On conditions for the vernal blooming of phytoplankton. J Cons Int Explor Mer 18:287-295

Toyoda T, Okamoto S (2017) Physical forcing of late summer chlorophyll a blooms in the oligotrophic eastern North Pacific. Journal of Geophysical Research: Oceans 122:1849-1861

Venrick E (1993) Phytoplankton seasonality in the central North Pacific: the endless summer reconsidered. Limnology and Oceanography 38:1135-1149

Villareal TA, et al. (2011) Summer Blooms of Diatom-Diazotroph Assemblages and Surface Chlorophyll in the North Pacific Gyre: A Disconnect. Journal of Geophysical Research: Oceans 116

White AE, Spitz YH, Letelier RM (2007) What factors are driving summer phytoplankton blooms in the North Pacific Subtropical Gyre? Journal of Geophysical Research: Oceans 112

Wilson C (2003) Late Summer Chlorophyll Blooms in the Oligotrophic North Pacific Subtropical Gyre. Geophysical Research Letters 30

Wilson C (2011) Chlorophyll Anomalies along the Critical Latitude at 30°N in the NE Pacific. Geophysical Research Letters 38

Wilson C (2021) Evidence of Episodic Nitrate Injections in the Oligotrophic North Pacific Associated With Surface Chlorophyll Blooms. Journal of Geophysical Research: Oceans 126:e2021JC017169

Wilson C, Coles VJ (2005) Global climatological relationships between satellite biological and physical observations and upper ocean properties. Journal of Geophysical Research: Oceans 110

Wilson C, et al. (2013) Chlorophyll Bloom Development and the Subtropical Front in the North Pacific. Journal of Geophysical Research: Oceans 118:1473 - 1488

Wilson C, et al. (2008) Biological and Physical Forcings of Late Summer Chlorophyll Blooms at 30°N in the Oligotrophic Pacific. Journal of Marine Systems 69:164 - 176

Wilson ST, Hawco NJ, Armbrust EV, Barone B, Björkman KM, Boysen AK, Burgos M, Burrell TJ, Casey JR, DeLong EF, Dugenne M, Dutkiewicz S, Dyhrman ST, Ferrón S, Follows MJ, Foreman RK, Funkey CP, Harke MJ, Henke BA, Hill CN, Hynes AM, Ingalls AE, Jahn O, Kelly RL, Knapp AN, Letelier RM, Ribalet F, Shimabukuro EM, Tabata RKS, Turk-Kubo KA, White AE, Zehr JP, John S, Karl DM (2019) Kīlauea lava fuels phytoplankton bloom in the North Pacific Ocean. Science 365:1040-1044